Second-Kind Boundary Integral Equations for Scattering at Composite Partly Impenetrable Objects

Xavier Claeys, Ralf Hiptmair, Elke Spindler

ETH
Eidgenössische Technische Hochschule Zürich
Swiss Federal Institute of Technology Zurich

Seminar for Applied Mathematics SAM

Second-Kind Boundary Integral Equations for Scattering at Composite Partly Impenetrable Objects

X. Claeys and R. Hiptmair and E. Spindler

Research Report No. 2015-19
June 2015

Seminar für Angewandte Mathematik
Eidgenössische Technische Hochschule
CH-8092 Zürich
Switzerland

Funding SNF: 20021_137873/1

Second-Kind Boundary Integral Equations for Scattering at Composite Partly Impenetrable Objects

Xavier Claeys[*†‡], **Ralf Hiptmair**[◇], **and Elke Spindler**[◇]

June 11, 2015

Abstract We consider acoustic scattering of time-harmonic waves at objects composed of several homogeneous parts. Some of those may be impenetrable, giving rise to Dirichlet boundary conditions on their surfaces. We start from the second-kind boundary integral approach of [X. Claeys, and R. Hiptmair, and E. Spindler. *A second-kind Galerkin boundary element method for scattering at composite objects.* BIT Numerical Mathematics, 55(1):33-57, 2015] and extend it to this setting. Based on so-called global multi-potentials, we derive variational second-kind boundary integral equations posed in $L^2(\Sigma)$, where Σ denotes the union of material interfaces. To suppress spurious resonances, we introduce a combined-field version (CFIE) of our new method.

Thorough numerical tests highlight the low and mesh-independent condition numbers of Galerkin matrices obtained with discontinuous piecewise polynomial boundary element spaces. They also confirm competitive accuracy of the numerical solution in comparison with the widely used first-kind single-trace approach.

Keywords Acoustic scattering, second-kind boundary integral equations, Galerkin boundary element methods

Mathematics Subject Classification (2000) 65N12, 65N38, 65R20

[*] Sorbonne Universités, UPMC Univ Paris 06, UMR 7598, Laboratoire Jacques-Louis Lions, F-75005, Paris, France,
[†] CNRS, UMR 7598, Laboratoire Jacques-Louis Lions, F-75005, Paris, France,
[‡] INRIA-Paris-Rocquencourt, EPC Alpines, Domaine de Voluceau, BP105, F-78153 Le Chesnay Cedex, email: xavier.claeys@upmc.fr,
[◇] Seminar for Applied Mathematics, Swiss Federal Institute of Technology, Zurich, Switzerland, emails: {hiptmair,elke.spindler}@sam.math.ethz.ch. The work of E. Spindler was partially supported by SNF under grant 20021_137873/1.

1 Introduction

1.1 Acoustic Scattering Boundary Value Problem

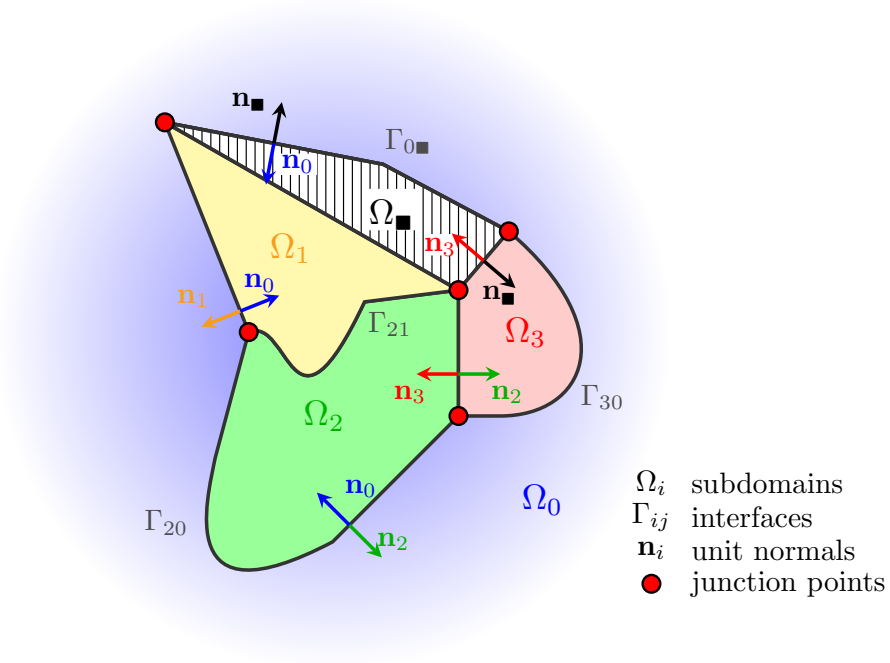

Fig. 1.1: Two-dimensional illustration of a typical geometry of a composite scatterer for $N = 3$.

The governing equation for acoustic scattering of time-harmonic waves is the Helmholtz equation. In this article, we confine ourselves to the case where we have a homogeneous diffusion coefficient, i.e. there is no spatial dependence of the second-order coefficient.

We define a partitioning of the bounded domain $\Omega_* \subset \mathbb{R}^d$, $d = 2, 3$, occupied by the scatterer, into open Lipschitz subdomains, i.e. $\overline{\Omega}_* = \big(\cup_{i=1}^N \overline{\Omega}_i\big) \cup \overline{\Omega}_\blacksquare$, where $\overline{\Omega}$ denotes the closure of the domain Ω. The subdomains $\Omega_1, \ldots, \Omega_N$ represent the different homogeneous penetrable materials and the impenetrable object with Lipschitz curvilinear polygonal/polyhedral boundary is given by $\Omega_\blacksquare$. See Figure 1.1 for a drawing of the scatterer in the case $d = 2$. The unbounded exterior complement of the scatterer is given by the Lipschitz domain $\Omega_0 := \mathbb{R}^d \setminus \overline{\Omega}_*$. Like $\Omega_1, \ldots, \Omega_N$, it represents a homogeneous penetrable material. We characterise the penetrable materials by their constant wave numbers $\kappa_i \in \mathbb{R}_+$, for $i \in \{0, 1, \ldots, N\}$. Hence, the resulting global coefficient function $\kappa \in L^\infty(\mathbb{R}^d)$, $\kappa\big|_{\Omega_i} \equiv \kappa_i$ is piecewise constant.

The impenetrable object $\Omega_\blacksquare$ will be modeled by imposing Dirichlet boundary conditions at its boundary $\partial\Omega_\blacksquare$.

By construction, we observe that $\Omega_i \cap \Omega_j = \varnothing$ for $j \neq i$, for indices $i, j \in \{\blacksquare, 0, 1, \ldots, N\}$. The boundary of the subdomain Ω_i is given by $\partial\Omega_i$ for $i \in \{\blacksquare, 0, 1 \ldots, N\}$. For Lipschitz domains, and in particular for each Ω_i, there exists a unit normal vector field $\mathbf{n}_i$ on $\partial\Omega_i$, $\mathbf{n}_i : \partial\Omega_i \to \mathbb{R}^d$, pointing towards the exterior of Ω_i.

The interface between two subdomains Ω_i and Ω_j is denoted by $\Gamma_{ij} := \partial\Omega_i \cap \partial\Omega_j$. Moreover, we introduce the so-called skeleton $\Sigma := \bigcup_{i=0}^{N} \partial\Omega_i$, the union of all boundaries of penetrable objects.

Sources in our scattering model are given through an *incident wave*, coming from infinity and impinging on the scattering obstacle. We assume that the source $U_{\text{inc}} \in C^\infty(\mathbb{R}^d)$[1] satisfies the Helmholtz equation

$$-\Delta U_{\text{inc}} - \kappa_0^2 U_{\text{inc}} = 0 \quad \text{everywhere in } \mathbb{R}^d\,, \tag{1.1}$$

where κ_0 denotes the wave number corresponding to the exterior unbounded domain Ω_0.

The acoustic scattering problem with impenetrable parts looks for $U \in H^1_{0,\text{loc}}(\mathbb{R}^d \setminus \Omega_\blacksquare)$ such that[2]

$$\int_{\mathbb{R}^d \setminus \overline{\Omega}_\blacksquare} \mathbf{grad}\, U(\boldsymbol{x}) \cdot \mathbf{grad}\, V(\boldsymbol{x}) - \kappa^2(\boldsymbol{x}) U(\boldsymbol{x}) V(\boldsymbol{x})\, \mathrm{d}\boldsymbol{x} = 0\,, \tag{1.2a}$$

for all $V \in H^1_{0,\text{comp}}(\mathbb{R}^d \setminus \Omega_\blacksquare)$, and the scattered field $U_s := U - U_{\text{inc}}$ satisfies the *Sommerfeld radiation condition* [12, Sect. 2.2]

$$\lim_{r\to\infty} \int_{|\boldsymbol{x}|=r} \left| \mathbf{grad}\, U_s(\boldsymbol{x}) \cdot \frac{\boldsymbol{x}}{|\boldsymbol{x}|} - \mathrm{i}\kappa_0 U_s(\boldsymbol{x}) \right|^2 \mathrm{d}S(\boldsymbol{x}) = 0\,. \tag{1.2b}$$

Existence and uniqueness of solutions of (1.2) is well established [2, 20].

1.2 Well-Established Second-Kind Boundary Integral Formulations

Boundary integral equations (BIE) are an effective tool to model the acoustic scattering of waves at partly impenetrable objects consisting of several homogeneous materials. They form the foundation for Galerkin boundary element methods (BEM), a popular class of methods to discretise and numerically compute acoustic fields. BEM are – in contrast to finite element methods

[1] Capital letters are used to refer to functions defined over a volume domain.

[2] Notations for function spaces (Sobolev spaces) follow the usual conventions, see [9, 26]. In particular, we write $H^s_{\text{loc}}(\mathbb{R}^d)$ for functions that belong to $H^s(K)$ for any compact subset K of $\mathbb{R}^d$, see [33, Definition 2.6.1]. $H^s_{\text{comp}}(\Omega)$ contains all distributions in $H^s_{\text{loc}}(\Omega)$ that have compact support in Ω, see [33, Definition 2.6.5] and $H^1_{0,\text{loc}}(\Omega)$ consists of all distributions in $H^s_{\text{loc}}(\Omega)$ that vanish on $\partial\Omega$.

– well-suited for scattering problems, since they can easily treat unbounded domains. Already very well-established are second-kind BIE for transmission problems in the case of a homogeneous scatterer, i.e. when there is no impenetrable object $\Omega_{\blacksquare}$ and $N = 1$ (see [25, 28, 32] or [12, Sect. 3] or [33, Sect. 3.9]). Also well understood are second-kind BIE for exterior Dirichlet problems (c.f. [12, Sect. 3] or [33, Sect. 3.9], [14,15]), i.e. the case described in Subsection 1.1 for $N = 0$. In this case, the occurance of spurious resonances is a persistent problem and combined field integral equations (CFIE) are a well-established tool to overcome the issue (see [3, 4]).

Our aim is to unify these approaches to treat complex scatterers consisting of impenetrable as well as several penetrable homogeneous materials.

1.3 Related Work

For the geometric situation described in Subsection 1.1, a widely used BIE is the so-called first-kind single-trace formulation (STF) [13, 35], in computational electromagnetics also known as Poggio-Miller-Chew-Harrington-Wu-Tsai (PMCHWT) integral equation [5, 19, 31, 36]. Other recently developed approaches to solve the same type of problems are various kinds of multi-trace formulations (MTF), see [7–10, 22, 29, 30]. The Galerkin discretisation of the classical first-kind STF as well as of the MTF leads to ill-conditioned linear systems on fine meshes and no operator preconditioner [21] ("Calderón preconditioning") is available yet in the case of the classical single-trace approach. In the case of the MTF, Calderón preconditioning is applicable (see [9, Sect. 4]).

We have developed a formulation, the so-called second-kind STF, proposed and analyzed in [6], further developed in [11] as well as in [17], extending earlier work for a single homogeneous scatterer [25, 28, 32], that yields *intrinsically well-conditioned linear systems*. This type of STF is based on so-called multipotentials (see Subsection 2.2).

1.4 Novelty and Outline

In this article, we extend the Galerkin BEM approach for second-kind STF for transmission problems presented in [11] to partly impenetrable objects. It turns out that also in this case it is still possible to pose the second-kind STF in L^2 (cf. Section 3.1). Special emphasis is put on the algorithmic details of our proposed method. Theoretical considerations will only be recalled briefly and for proofs we largely refer to [6, 11].

To overcome spurious resonances, we adopt the idea of (direct) combined field integral equations (CFIE, see [3, 4]) in Section 4. Numerical tests in three dimensions provide solid evidence for stability of our second-kind Galerkin discretisation as well as mesh size independent conditioning of the linear systems and show competitive accuracy in comparison with the classical STF.

We emphasize that the focus of the present work is not on theoretical investigations, but on the derivation of the new boundary integral equations, the implementation of the related Galerkin BEM, and numerical tests probing specific properties in typical settings. In Section 2 we present the basic tools, set up the notation, and introduce the spaces needed for our second-kind single-trace formulation. In Section 3 we present the formulation itself and afterwards in Section 4, we discuss its CFIE extension. Based on a concrete example, the discretisation and implementation of the method is discussed in Section 5. Finally, we present the numerical results in Section 6.

2 Boundary Integral Equations

2.1 Traces and Potentials

We are going to use the same notation as introduced in [11, Subsection 3.1]. For the ith subdomain, $i \in \{\blacksquare, *, 0, 1, \dots, N\}$, we introduce the *interior Dirichlet trace* $\gamma_D^i : H^1_{\mathrm{loc}}(\Omega_i) \to H^{\frac{1}{2}}(\partial\Omega_i)$, extending the pointwise restriction of smooth functions to $\partial\Omega_i$, and the *interior Neumann trace* (co-normal trace), $\gamma_N^i : H^1_{\mathrm{loc}}(\Delta, \overline{\Omega}_i) \to H^{-\frac{1}{2}}(\partial\Omega_i)$, $\gamma_N^i := \mathbf{n}_i \cdot \binom{\gamma_D^i}{\gamma_D^i} \circ \mathbf{grad}$, *cf.*, e.g., [33, Theorems 2.6.9, 2.8.3 & Lemma 2.8.4].[3] The *exterior Dirichlet and Neumann* traces are defined by $\gamma_D^{i,c} : H^1_{\mathrm{loc}}(\mathbb{R}^d \setminus \overline{\Omega}_i) \to H^{\frac{1}{2}}(\partial\Omega_i)$ and $\gamma_N^{i,c} : H^1_{\mathrm{loc}}(\Delta, \mathbb{R}^d \setminus \Omega_i) \to H^{-\frac{1}{2}}(\partial\Omega_i)$, $\gamma_N^i := \mathbf{n}_i \cdot \binom{\gamma_D^{i,c}}{\gamma_D^{i,c}} \circ \mathbf{grad}$, respectively.

The associated trace spaces, henceforth called "Dirichlet trace space" and "Neumann trace space", can be merged into the "Cauchy trace space"

$$\mathcal{H}(\partial\Omega_i) := H^{\frac{1}{2}}(\partial\Omega_i) \times H^{-\frac{1}{2}}(\partial\Omega_i)\,, \tag{2.1}$$

which is *self-dual* with respect to the pairing[4]

$$\langle\!\langle \mathfrak{u}, \mathfrak{v} \rangle\!\rangle_{\mathcal{H}(\partial\Omega_i)} := \langle u, \varphi \rangle_{\partial\Omega_i} - \langle v, \nu \rangle_{\partial\Omega_i}\,,\ \mathfrak{u} := \begin{pmatrix} u \\ \nu \end{pmatrix},\ \mathfrak{v} := \begin{pmatrix} v \\ \varphi \end{pmatrix} \in \mathcal{H}(\partial\Omega_i)\,, \tag{2.2}$$

with $\langle \cdot, \cdot \rangle_{\Omega_i}$ denoting (extensions of) the L^2-duality pairing on $\partial\Omega_i$. A related compact notation is the Cauchy trace operator

$$\gamma^i : H^1_{\mathrm{loc}}(\Delta, \Omega_i) \to \mathcal{H}(\partial\Omega_i)\,, \quad \gamma^i U := \begin{pmatrix} \gamma_D^i U \\ \gamma_N^i U \end{pmatrix}. \tag{2.3}$$

Potential representations of solutions of (1.2) are the first step towards boundary integral equations. The following result can be found in [33, Sect. 3.11] and [26, Ch. 6]:

[3] $H^1_{\mathrm{loc}}(\Delta, \overline{\Omega}) := \{U \in H^1_{\mathrm{loc}}(\overline{\Omega}) \,|\, \Delta U \in L^2_{\mathrm{comp}}(\overline{\Omega})\}$, see [33, Equation (2.108)].

[4] Fraktur font is used to designate functions in the Cauchy trace space, where Roman typeface is reserved for Dirichlet traces, and Greek symbols for Neumann traces.

Lemma 2.1 (Single Domain Representation Formula) *There are continuous linear operators, depending on the constant $\kappa > 0$, the*

$$\begin{aligned} \text{single layer potential} \quad & \mathbb{S}_i[\kappa] : H^{-\frac{1}{2}}(\partial\Omega_i) \to H^1_{\mathrm{loc}}(\Delta, \mathbb{R}^d \setminus \partial\Omega_i) \,, \\ \text{double layer potential} \quad & \mathbb{D}_i[\kappa] : H^{\frac{1}{2}}(\partial\Omega_i) \to H^1_{\mathrm{loc}}(\Delta, \mathbb{R}^d \setminus \partial\Omega_i) \,, \end{aligned}$$

such that

(i) $\mathbb{S}_i[\kappa](\varphi)$ *and* $\mathbb{D}_i[\kappa](u)$ *satisfy* $-\Delta \cdot - \kappa^2 \cdot = 0$ *in* Ω_i *and in* $\mathbb{R}^d \setminus \overline{\Omega_i}$. *They also satisfy the Sommerfeld radiation conditions* (1.2b) *for any* $\varphi \in H^{-\frac{1}{2}}(\partial\Omega_i)$, $u \in H^{\frac{1}{2}}(\partial\Omega_i)$.

(ii) Every solution $U \in H^1_{\mathrm{loc}}(\Omega_i)$ *of* $\left(-\Delta - \kappa^2\right) U = 0$ *that satisfies the Sommerfeld radiation conditions* (1.2b), *if* $i = 0$, *fulfills*

$$\mathbb{G}_i[\kappa](\gamma^i U) = \begin{cases} U & \text{on } \Omega_i \,, \\ 0 & \text{on } \mathbb{R}^d \setminus \overline{\Omega_i} \,, \end{cases} \tag{2.4}$$

with the local potentials *defined by*

$$\mathbb{G}_i[\kappa](\mathfrak{u}) := -\mathbb{D}_i[\kappa](u) + \mathbb{S}_i[\kappa](\varphi) \,, \quad \mathfrak{u} := \begin{pmatrix} u \\ \varphi \end{pmatrix} \in \mathcal{H}(\partial\Omega_i) \,.$$

For distributions φ and u on $\partial\Omega_i$ the potentials possess the integral representations

$$\begin{aligned} \mathbb{S}_i[\kappa](\varphi)(\boldsymbol{x}) &= \int_{\partial\Omega_i} \Phi_\kappa(\boldsymbol{x} - \boldsymbol{y})\, \varphi(\boldsymbol{y})\, \mathrm{d}S(\boldsymbol{y}) \,, \\ \mathbb{D}_i[\kappa](u)(\boldsymbol{x}) &= \int_{\partial\Omega_i} \mathbf{grad}_{\boldsymbol{y}}\, \Phi_\kappa(\boldsymbol{x} - \boldsymbol{y}) \cdot \mathbf{n}_i(\boldsymbol{y})\, u(\boldsymbol{y})\, \mathrm{d}S(\boldsymbol{y}) \,, \end{aligned} \tag{2.5}$$

for $\boldsymbol{x} \notin \partial\Omega_i$, with the fundamental solutions

$$\Phi_\kappa(\boldsymbol{z}) = \begin{cases} \frac{\mathrm{i}}{4} H_0^{(1)}(\kappa\,|\boldsymbol{z}|), & d = 2 \\ \frac{1}{4\pi|\boldsymbol{z}|} \exp(\mathrm{i}\kappa\,|\boldsymbol{z}|), & d = 3 \end{cases} , \quad \kappa \in \mathbb{R}_+ \,, \tag{2.6}$$

where $H_0^{(1)}$ is the Hankel function of the first kind and $|\cdot|$ represents the Euclidean norm.

Notations. For simplicity we neglect the argument $[\kappa]$ in $\mathbb{S}_i[\kappa]$, $\mathbb{D}_i[\kappa]$, and $\mathbb{G}_i[\kappa]$ and write $\mathbb{S}_i := \mathbb{S}_i[\kappa_i]$, $\mathbb{D}_i := \mathbb{D}_i[\kappa_i]$, $\mathbb{G}_i := \mathbb{G}_i[\kappa_i]$, respectively, in the cases where κ in the formulas (2.5) coincides with the local wave number κ_i of Ω_i, $i \in \{0, 1, \ldots, N\}$.

2.2 Skeleton Trace Spaces and Multi-potentials

This subsection will follow the same notation as introduced in [11, Subsections 3.2, 3.3] or [6, Section 2], but will extend it to the setting with impenetrable parts.

Definition 2.1 (Multi-Trace Space [6, Section 2], [11, Def. 3.1]) The skeleton *multi-trace space* is defined as the product of local Cauchy trace spaces

$$\boldsymbol{\mathcal{MT}}(\Sigma) := \prod_{i=0}^{N} \mathcal{H}(\partial\Omega_i) \,. \tag{2.7}$$

The skeleton multi-trace operator γ^{Σ}, mapping $H^1_{\mathrm{loc}}(\Delta, \mathbb{R}^d \setminus \Omega_{\blacksquare})$ into the multi-trace space is given by $\gamma^{\Sigma} : H^1_{\mathrm{loc}}(\Delta, \mathbb{R}^d \setminus \Omega_{\blacksquare}) \to \boldsymbol{\mathcal{MT}}(\Sigma)$,

$$U := (\gamma^0 U, \gamma^1 U, ..., \gamma^N U) \,. \tag{2.8}$$

We take any $\mathfrak{u} = (\mathfrak{u}_0, ..., \mathfrak{u}_N)$, $\mathfrak{v} = (\mathfrak{v}_0, ..., \mathfrak{v}_N) \in \boldsymbol{\mathcal{MT}}(\Sigma)$ and obtain self-duality of $\boldsymbol{\mathcal{MT}}(\Sigma)$ by the L^2-type bilinear pairing (2.2) defined as

$$\langle\!\langle \mathfrak{u}, \mathfrak{v} \rangle\!\rangle := \sum_{i=0}^{N} \langle\!\langle \mathfrak{u}_i, \mathfrak{v}_i \rangle\!\rangle_{\mathcal{H}(\partial\Omega_i)} \,. \tag{2.9}$$

For sufficiently smooth functions we can rewrite (2.9) using the fact that each transmission-interface is visited twice and each impenetrable interface is visited once when summing integrals over all subdomain boundaries:

$$\langle\!\langle \mathfrak{u}, \mathfrak{v} \rangle\!\rangle = \sum_{0 \le j < i \le N} \int_{\Gamma_{ij}} u_i \psi_i - \nu_i v_i + u_j \psi_j - \nu_j v_j \,\mathrm{d}S + \sum_{0 \le i \le N} \int_{\Gamma_{i\blacksquare}} u_i \psi_i - \nu_i v_i \,\mathrm{d}S \,, \tag{2.10}$$

where $\mathfrak{u}_i = (u_i, \nu_i)$, $\mathfrak{v}_i = (v_i, \psi_i)$. Next, we introduce the important subspace of unique traces in $\boldsymbol{\mathcal{MT}}(\Sigma)$ that incorporates homogeneous Dirichlet boundary conditions at $\partial\Omega_{\blacksquare}$.

Definition 2.2 (Single-Trace Space [6, Section 2], [11, Def. 3.2])

$$\boldsymbol{\mathcal{ST}}(\Sigma) := \Big\{ (u_0, \nu_0, \ldots, u_N, \nu_N) \in \boldsymbol{\mathcal{MT}}(\Sigma) \,:\, \exists U \in H^1_0(\mathbb{R}^d \setminus \Omega_{\blacksquare}),$$
$$u_i = \gamma^i_D U,\ \exists \boldsymbol{\phi} \in \boldsymbol{H}(\mathrm{div}, \mathbb{R}^d \setminus \Omega_{\blacksquare}),\ \nu_i = \boldsymbol{n}_i \cdot \begin{pmatrix} \gamma^i_D \\ \gamma^i_D \end{pmatrix} \boldsymbol{\phi},\ \forall i \in \{0, \ldots, N\} \Big\} \,.$$

We observe that functions in $\boldsymbol{\mathcal{ST}}(\Sigma)$ are skeleton traces of functions defined everywhere on $\mathbb{R}^d \setminus \overline{\Omega}_{\blacksquare}$. Moreover, the *transmission conditions* inherent in the variational formulation (1.2a) imply that the solution U of (1.2) is an element of $\boldsymbol{\mathcal{ST}}(\Sigma)$:

$$U \text{ solves (1.2a)} \quad \Rightarrow \quad \gamma^{\Sigma} U \in \boldsymbol{\mathcal{ST}}(\Sigma) \,. \tag{2.11}$$

The "polar set" characterisation of $\boldsymbol{\mathcal{ST}}(\Sigma)$ as a subspace of $\boldsymbol{\mathcal{MT}}(\Sigma)$, see also [6, Prop. 2.1], [9, Thm. 3.1] and [11], still holds for our extension to impenetrable parts.

$$\boldsymbol{\mathcal{ST}}(\Sigma) = \{\mathfrak{u} \in \boldsymbol{\mathcal{MT}}(\Sigma) : \langle\langle \mathfrak{u}, \mathfrak{v} \rangle\rangle = 0, \ \forall \mathfrak{v} \in \boldsymbol{\mathcal{ST}}(\Sigma)\} . \tag{2.12}$$

Based on the spaces introduced above, we define the so-called multi-potential.

Definition 2.3 (Multi-Potential [6, Section 5], [11, Def. 3.3]) The *multi-potential* is defined as the sum of all local potentials $\mathbb{G}_i[\kappa_i]$ defined in Lemma 2.1, $i = 0, ..., N$:

$$\mathbb{M}_\Sigma : \boldsymbol{\mathcal{MT}}(\Sigma) \to H^1_{\mathrm{loc}}(\Delta, \mathbb{R}^d \setminus \Sigma), \quad \mathbb{M}_\Sigma(\mathfrak{u}) := \sum_{i=0}^{N} \mathbb{G}_i[\kappa_i](\mathfrak{u}_i) . \tag{2.13}$$

In the case of an incident field, an immediate consequence of equation (2.4) applied to the multi-potential is

Corollary 2.1 (Global Representation Formula [11, Cor. 3.1]) *Let U solve the transmission problem (1.2), then*

$$U - \chi_{\Omega_0} U_{\mathrm{inc}} = \mathbb{M}_\Sigma(\gamma^\Sigma U - \mathfrak{u}^0_{\mathrm{inc}}) , \tag{2.14}$$

where γ^Σ is the multi-trace defined in (2.8), χ_{Ω_0} is the characteristic function of Ω_0, and $\mathfrak{u}^0_{\mathrm{inc}} := (\gamma^0 U_{\mathrm{inc}}, 0, \ldots, 0)$.

3 Second-kind Boundary Integral Equations

Following the lines of [11, Subsection 3.3], we define the boundary integral operator $\mathbf{M}_\Sigma$ by taking the skeleton trace of (2.13).

Definition 3.1 (Multi Boundary Integral Operator [11, Def. 3.4])

$$\mathbf{M}_\Sigma := \gamma^\Sigma \mathbb{M}_\Sigma : \quad \boldsymbol{\mathcal{MT}}(\Sigma) \quad \to \quad \boldsymbol{\mathcal{MT}}(\Sigma) . \tag{3.1}$$

Notations. If $\mathbb{M}_\Sigma$ or $\mathbf{M}_\Sigma$ are supplied with an argument $[\kappa]$, all wave numbers κ_i in (2.13) and (3.1) are supposed to agree with κ in $\mathbb{M}_\Sigma[\kappa]$ and $\mathbf{M}_\Sigma[\kappa]$, respectively.

The representation formula in (2.14) paves the way to the boundary integral formulation. We take the skeleton-trace on both sides of the equation, test the resulting equation with $\mathfrak{v} \in \boldsymbol{\mathcal{MT}}(\Sigma)$ and integrate over the skeleton Σ. Finally, we obtain the following variational BIE satisfied by $\mathfrak{u} := \gamma^\Sigma U$.

Formulation 3.1 *Search* $\mathfrak{u} \in \boldsymbol{\mathcal{ST}}(\Sigma)$:

$$\langle\!\langle (\mathsf{Id} - \mathsf{M}_\Sigma)\mathfrak{u}, \mathfrak{v} \rangle\!\rangle = \langle\!\langle \mathfrak{u}_{\mathrm{inc}}, \mathfrak{v} \rangle\!\rangle \,, \quad \forall \mathfrak{v} \in \boldsymbol{\mathcal{MT}}(\Sigma), \tag{3.2}$$

where $\mathfrak{u}_{\mathrm{inc}} := \gamma^\Sigma U_{\mathrm{inc}}$.

The simple expression on the right hand side is due to the identity

$$\langle\!\langle (\mathsf{Id} - \mathsf{M}_\Sigma)\mathfrak{u}^0_{\mathrm{inc}}, \mathfrak{v} \rangle\!\rangle = \langle\!\langle \mathfrak{u}_{\mathrm{inc}}, \mathfrak{v} \rangle\!\rangle \,.$$

The identity holds, since we assume that the incident wave U_{inc} solves an interior Helmholtz problem on Ω_*, see (1.1). To be more precise, by (2.4), we obtain

$$\mathbb{G}_*[\kappa_0](\gamma^* U_{\mathrm{inc}}) = \begin{cases} U_{\mathrm{inc}} & \text{on } \Omega_* \,, \\ 0 & \text{on } \mathbb{R}^d \backslash \overline{\Omega_*} \,. \end{cases} \tag{3.3}$$

Since $\Omega_0 = \mathbb{R}^d \setminus \overline{\Omega}_*$, taking into account the jump relations [33, Thm. 3.3.1] together with the fact that

$$\gamma^* U_{\mathrm{inc}} = \begin{pmatrix} \gamma^0_D \\ -\gamma^0_N \end{pmatrix} U_{\mathrm{inc}}$$

and the definition of the multi boundary integral operator 3.1, we observe

$$\begin{aligned} \mathsf{M}_\Sigma\, \mathfrak{u}^0_{\mathrm{inc}} &= \gamma^\Sigma \mathbb{G}_0[\kappa_0](\gamma^0 U_{\mathrm{inc}}) \\ &= -\gamma^\Sigma \mathbb{G}_*[\kappa_0](\gamma^* U_{\mathrm{inc}}) \\ &\overset{(3.3)}{=} -(0, 0, \gamma^1 U_{\mathrm{inc}}, \ldots, \gamma^N U_{\mathrm{inc}}) \,, \end{aligned}$$

which finally leads to

$$(\mathsf{Id} - \mathsf{M}_\Sigma)\mathfrak{u}^0_{\mathrm{inc}} = \gamma^\Sigma U_{\mathrm{inc}} = \mathfrak{u}_{\mathrm{inc}} \,.$$

3.1 Second-Kind Boundary Integral Formulation in L^2

3.1.1 Formulation in L^2 Single-Trace Space

Formulation 3.1 remains well-defined in L^2-type function spaces. A justification for the pure transmission case can be found in [11, Lem. 3.2 and Sect. 4]. We will work with the L^2-version of the multi-trace space in (2.7).

Definition 3.2 (L^2 Multi-Trace Space [11, Def. 4.2]) The L^2 *skeleton multi-trace space* is given by

$$\boldsymbol{\mathcal{ML}}^2(\Sigma) := \prod_{i=0}^{N} L^2(\partial\Omega_i) \times L^2(\partial\Omega_i) \,. \tag{3.4}$$

Since the transmission conditions in L^2 reduce to interfacewise constraints on functions in the multi-trace space, it makes sense to define the lifted single-trace space in the following way.

Definition 3.3 (L^2 Single-Trace Space [11, Def. 4.2]) The L^2 *single-trace space* is defined by

$$\boldsymbol{\mathcal{SL}}^2(\Sigma) := \Big\{(u_0,\nu_0,\dots,u_N,\nu_N)\in\boldsymbol{\mathcal{ML}}^2(\Sigma):\quad u_i\big|_{\Gamma_{ij}} = u_j\big|_{\Gamma_{ij}},\\ \nu_i\big|_{\Gamma_{ij}} = -\nu_j\big|_{\Gamma_{ij}},\ \forall j<i \text{ and } u_i\big|_{\partial\Omega_\blacksquare}=0,\ \forall i\in\{0,\dots,N\}\Big\}.$$

Of course, the polar identity (2.12) also holds in the L^2-setting. The proof works analogously to [11, Lemma 4.1].

Lemma 3.1

$$\boldsymbol{\mathcal{SL}}^2(\Sigma) = \{\mathbf{u}\in\boldsymbol{\mathcal{ML}}^2(\Sigma) : \langle\!\langle \mathbf{u},\mathbf{v}\rangle\!\rangle = 0,\ \forall \mathbf{v}\in\boldsymbol{\mathcal{SL}}^2(\Sigma)\}.$$

Taking any test function $\mathbf{v}\in\boldsymbol{\mathcal{SL}}^2(\Sigma)$, equation (3.2) will reduce to "0 = 0". It is a direct conclusion when combining the following Theorem 3.1 and the *polarity property* given in (2.12).

Theorem 3.1 (c.f. [6, Proposition 5.1] and [6, Theorem 4.2]) *For any tuple of wave numbers* $(\kappa_0,\kappa_1,\dots,\kappa_N)\in\mathbb{R}_+^{N+1}$*, it holds*

$$\langle\!\langle(\mathsf{Id}-\mathbf{M}_\kappa)\mathbf{u},\mathbf{v}\rangle\!\rangle = 0\ ,\ \forall\mathbf{u}\in\boldsymbol{\mathcal{ML}}^2(\Sigma),\ \forall\mathbf{v}\in\boldsymbol{\mathcal{SL}}^2(\Sigma). \tag{3.5}$$

Theorem 3.1 not only points to redundancy in the test space of the formulation, it also provides a remedy. Since $\boldsymbol{\mathcal{ST}}(\Sigma)$ is a closed subspace of $\boldsymbol{\mathcal{MT}}(\Sigma)$, it is sufficient to test with elements in *any* complement space $\boldsymbol{\mathcal{SL}}^{2,c}(\Sigma)$ of $\boldsymbol{\mathcal{SL}}^2(\Sigma)\subset\boldsymbol{\mathcal{ML}}^2(\Sigma)$, i.e.,

$$\boldsymbol{\mathcal{ML}}^2(\Sigma) = \boldsymbol{\mathcal{SL}}^2(\Sigma)\oplus\boldsymbol{\mathcal{SL}}^{2,c}(\Sigma).$$

For the sake of easy implementation we choose $\boldsymbol{\mathcal{SL}}^{2,c}(\Sigma) := \boldsymbol{\mathcal{SL}}^{2,\perp}(\Sigma)$, the L^2-orthogonal complement space, which has a simple characterisation.

Definition 3.4 (Orth. Complement of the Single-Trace L^2-Space)

$$\boldsymbol{\mathcal{SL}}^{2,\perp}(\Sigma) := \Big\{(u_0,\nu_0,\dots,u_N,\nu_N)\in\boldsymbol{\mathcal{ML}}^2(\Sigma):\quad u_i\big|_{\Gamma_{ij}} = -u_j\big|_{\Gamma_{ij}},\\ \nu_i\big|_{\Gamma_{ij}} = \nu_j\big|_{\Gamma_{ij}},\ j<i \text{ and } \nu_i\big|_{\partial\Omega_\blacksquare}=0,\ \forall i\in\{0,1,\dots,N\}\Big\}.$$

In combination with Theorem 3.1, it suggests the following variational BIE, which is equivalent to Formulation 3.1.

Formulation 3.2 *Search* $\mathbf{u}\in\boldsymbol{\mathcal{SL}}^2(\Sigma)$:

$$\langle\!\langle(\mathsf{Id}-\mathbf{M}_\Sigma)\,\mathbf{u},\mathbf{v}\rangle\!\rangle = \langle\!\langle\mathbf{u}_{\mathrm{inc}},\mathbf{v}\rangle\!\rangle\ ,\quad \forall\mathbf{v}\in\boldsymbol{\mathcal{SL}}^{2,\perp}(\Sigma). \tag{3.6}$$

By construction the following corollary holds true:

Corollary 3.1 *Formulation 3.2 is consistent with the original scattering problem in the sense that the exact solution of (1.2) will also fulfill Formulation 3.2.*

Making use of elliptic lifting results [24, Theorem B.2], [18, Remark 2.4.6, Corollary 2.6.7], we observe that for the solution of (1.2) it holds for some $\epsilon > 0$ that $U \in H^{\frac{3}{2}+\epsilon}_{\mathrm{loc}}(\mathbb{R}^d \setminus \Omega_\blacksquare)$. Thus, $\gamma^\Sigma U \in \boldsymbol{\mathcal{SL}}^2(\Sigma)$ and we can state the equivalence of Formulation 3.2 to the original problem (1.2).

Corollary 3.2 (Equivalence) *If Formulation 3.2 has a unique solution $\mathbf{u} \in \boldsymbol{\mathcal{SL}}^2(\Sigma)$, then $\mathbf{u}$ provides the multi-trace $\gamma^\Sigma U$ of the solution U of the original transmission problem (1.2).*

The proof of Corollary 3.2 is analogous to that of [11, Corollary 4.2].

Remark 3.1 [11, Thm. 4.1] provides the Fredholm property of the operator on the left hand side of equation (3.6) in the case when there is no impenetrable object. Hence, the proof of well-posedness of Formulation 3.2 reduces to the verification of

$$\mathrm{Ker}\,(\mathsf{Id} - \mathbf{M}_\Sigma) = \{0\}\,. \tag{3.7}$$

It is still open, whether (3.7) holds true. But numerical tests (see [11, Subsection 6.1]) indicate the absence of spurious resonances in the case without impenetrable parts. If impenetrable parts are present, spurious resonances can occur for particular wave numbers. A remedy will be devised in Section 4.

3.1.2 Formulation in L^2 Skeleton Trace Space

For implementation it is useful to consider the L^2 skeleton space.

Definition 3.5 (L^2 Skeleton Space) The *L^2 skeleton space* is given by

$$\boldsymbol{\mathcal{L}}^2(\Sigma) := \left(\prod_{0\le j<i\le N} L^2(\Gamma_{ij}) \times L^2(\Gamma_{ij})\right) \times \left(\prod_{0\le i\le N} \{0\} \times L^2(\Gamma_{i\blacksquare})\right).$$

It is isomorphic to $\boldsymbol{\mathcal{SL}}^2(\Sigma)$ by the following one-to-one correspondance. Any element $\mathbf{u} = (u_{ij}, \nu_{ij})_{j<i} \in \boldsymbol{\mathcal{L}}^2(\Sigma)$ is associated to the element $\mathcal{I}(\mathbf{u}) = (u_0, \nu_0, \ldots, u_N, \nu_N) \in \boldsymbol{\mathcal{SL}}^2(\Sigma)$ with

$$(u_i, \nu_i) = \begin{cases} (u_{ij}, \nu_{ij}) & \text{on } \Gamma_{ij} \text{ if } i > j \ge 0 \\ (u_{ji}, -\nu_{ji}) & \text{on } \Gamma_{ji} \text{ if } 0 \le i < j \\ (u_{i\blacksquare} \equiv 0, \nu_{i\blacksquare}) & \text{on } \Gamma_{i\blacksquare} \end{cases}, \; i = 0, \ldots, N\,. \tag{3.8}$$

In a similar manner, we find an isomorphism between $\boldsymbol{\mathcal{SL}}^{2,\perp}(\Sigma)$ and $\boldsymbol{\mathcal{L}}^2(\Sigma)$. In comparison to (3.8), when going from $\boldsymbol{\mathcal{L}}^2(\Sigma)$ to $\boldsymbol{\mathcal{SL}}^{2,\perp}(\Sigma)$, the idea is to flip the role Dirichlet data u_{ij} and Neumann data ν_{ij}. Any element $\mathbf{u} =$

$(u_{ij},\nu_{ij})_{j<i} \in \boldsymbol{\mathcal{L}}^2(\Sigma)$ is associated to the element $\mathcal{J}(\mathfrak{u}) = (u_0,\nu_0,\dots,u_N,\nu_N) \in \boldsymbol{\mathcal{SL}}^{2,\perp}(\Sigma)$ via

$$(u_i,\nu_i) = \begin{cases} (-\nu_{ij},u_{ij}) & \text{on } \Gamma_{ij} \text{ if } i>j\geq 0 \\ (\nu_{ji},u_{ji}) & \text{on } \Gamma_{ji} \text{ if } 0\leq i<j \\ (-\nu_{i\blacksquare},u_{i\blacksquare}\equiv 0) & \text{on } \Gamma_{i\blacksquare} \end{cases}, \; i=0,\dots,N\,. \tag{3.9}$$

This leads to another Formulation equivalent to 3.2 with ansatz and test functions taken in $\boldsymbol{\mathcal{L}}^2(\Sigma)$, where $\mathcal{I}$ and $\mathcal{J}$ represent the action of the isomorphisms introduced above in (3.8) and (3.9), respectively.

Formulation 3.3 *Search* $\mathfrak{u} \in \boldsymbol{\mathcal{L}}^2(\Sigma)$:

$$\langle\!\langle (\mathsf{Id}-\mathbf{M}_\Sigma)\,\mathcal{I}(\mathfrak{u}),\mathcal{J}(\mathfrak{v})\rangle\!\rangle = \langle\!\langle \mathfrak{u}_{\mathrm{inc}},\mathcal{J}(\mathfrak{v})\rangle\!\rangle,\ \forall \mathfrak{v}\in\boldsymbol{\mathcal{L}}^2(\Sigma). \tag{3.10}$$

4 Combined Field Integral Equations

4.1 Impenetrable Scatterer

It is well-known that due to the presence of an impenetrable part, spurious resonances are observed in the case of a single impenetrable scatterer, i.e. $N=0$. A widely used method to overcome this issue are the so-called *combined field integral equations* based on an idea of Burton and Miller [4] (see also [3]). First, let us recall the direct CFIE policy for $N=0$. Later on, in Subsection 4.2, we will adapt the idea to the case of a composite scatterer.

For $U \in H^1_{0,\mathrm{loc}}(\mathbb{R}^d\setminus\Omega_\blacksquare)$, Calderón's identity is obtained by taking the trace $\gamma^\blacksquare$ or $\gamma^{\blacksquare,c}$ of Equation (2.14).

$$\gamma^{\blacksquare,c}U = \mathsf{P}_{\blacksquare,c}(\gamma^{\blacksquare,c}U)\,. \tag{4.1}$$

The operator $\mathsf{P}_{\blacksquare,c}$ is known as *Calderón projector*. They project boundary data from the Cauchy trace space $\mathcal{H}(\partial\Omega_\blacksquare)$ to the space of admissible boundary data, called *Cauchy data* $\mathcal{C}(\partial\Omega^c_\blacksquare)$ (see [33, Proposition 3.6.2]).

$$\begin{aligned}\mathcal{C}(\partial\Omega^c_\blacksquare) \coloneqq \{(u,\nu)^\top \in \mathcal{H}(\partial\Omega_\blacksquare) \,:\, &\exists U\in H^1_{\mathrm{loc}}(\mathbb{R}^d\setminus\Omega_\blacksquare) \text{ s.t.}\\ &\Delta U+\kappa_0^2U=0 \text{ in } \overline{\Omega}^c_\blacksquare, \text{ with } U \text{ satisfying Sommerfeld}\\ &\text{radiation conditions (1.2b) and } \gamma^{\blacksquare,c}U=(u,\nu)^\top\}\,.\end{aligned}$$

Proposition 3.6.2 in [33] tells us that we have

$$\mathfrak{u}\in\mathcal{C}(\partial\Omega^c_\blacksquare) \Leftrightarrow \mathfrak{u}=\mathsf{P}_{\blacksquare,c}\mathfrak{u}\,, \tag{4.2}$$

where the right hand side of the equivalence in (4.2) actually consists of two equations: the first equation corresponds to the Dirichlet trace and the second equation is related to the Neumann trace. Taking just one of the two equations to characterise the boundary data at impenetrable objects means that we loose information.

When solving the second-kind BIE, we rely on the second equation in (4.1), related to the Neumann trace. However, in the case when κ_0^2 is a Neumann eigenvalue of $-\Delta$, i.e. if

$$\Delta U + \kappa_0^2 U = 0 \text{ in } \Omega_\blacksquare\,,\ \gamma_N^\blacksquare U = 0\,, \tag{4.3}$$

has a nontrivial solution $U \in H^1_{\mathrm{loc}}(\Omega_\blacksquare)$, this second equation will fail to have a unique solution. We have to make use of both equations in (4.1).

The idea of CFIE is to use both equations in (4.1) in a complex linear combination. For this purpose we introduce the *trace transformation operator* Ψ that transfers Neumann to Dirichlet data and multiplies it by $\mathrm{i}\eta$, for some $\eta \in \mathbb{R} \setminus \{0\}$:

$$\begin{aligned} \Psi : \{0\} \times L^2(\partial\Omega_\blacksquare) &\to L^2(\partial\Omega_\blacksquare) \times \{0\}\,, \\ \mathfrak{v} = (0,\nu) &\mapsto \Psi(\mathfrak{v}) = \mathrm{i}\eta(\nu,0)\,. \end{aligned} \tag{4.4}$$

Then, the direct combined field integral approach corresponding to Formulation 3.3 in the case $N = 0$ boils down to the following variational problem:

Seek $\mathfrak{u} \in \{0\} \times L^2(\partial\Omega_\blacksquare)$ such that for all $\mathfrak{v} \in L^2(\partial\Omega_\blacksquare) \times \{0\}$, we have

$$\left\langle\!\!\left\langle \gamma^{\blacksquare,c}\,\mathbb{G}_0[\kappa_0]\mathfrak{u}, \Psi(\mathfrak{v}) + \mathfrak{v} \right\rangle\!\!\right\rangle_{\mathcal{H}(\partial\Omega_i)} = \left\langle\!\!\left\langle \gamma^{\blacksquare,c}\,U_{\mathrm{inc}}, \Psi(\mathfrak{v}) + \mathfrak{v} \right\rangle\!\!\right\rangle_{\mathcal{H}(\partial\Omega_i)}\,.$$

Splitting the boundary integral operator $\gamma^{\blacksquare,c}\,\mathbb{G}_0[\kappa_0]$ into components acting on individual traces, we find that this is actually equal to the direct CFIE of [3, 4].

4.2 Composite Scatterer

Our goal is to apply the same strategy as in Subsection 4.1 in the case of a composite scatterer. We are going to add the first equation of (4.1), related to the Dirichlet trace, as an additional term to (3.10). This will guarantee that there are no spurious resonances due to the impenetrable objects anymore.

Starting with the global representation formula (2.14) and using that the Dirichlet trace of the solution vanishes on the impenetrable boundary, we obtain for a solution U of (1.2):

$$\gamma_D^{\blacksquare,c}\,\mathbb{M}_\Sigma(\gamma^\Sigma U - \mathbf{u}^0_{\mathrm{inc}}) = \gamma_D^{\blacksquare,c}(U - \chi_{\Omega_0} U_{\mathrm{inc}}) = 0\,. \tag{4.5}$$

This equation represents the missing information, i.e. the first equation in (4.1), that we want to incorporate into Formulation 3.10. In order to be able to introduce the analogon to the trace transformation operator Ψ from Subsection 4.1, equation (4.4), we define the space $\widetilde{L^2}(\partial\Omega_\blacksquare)$, which is given by the extension of $L^2(\partial\Omega_\blacksquare)$ by zero to

$$\left(\prod_{0\le j<i\le N} \{0\} \times \{0\}\right) \times \left(\prod_{0\le i\le N} \{0\} \times L^2(\Gamma_{i\blacksquare})\right)\,.$$

For some fixed $\eta \in \mathbb{R} \setminus \{0\}$ we define the trace transformation operator

$$\begin{aligned} \Psi &: \boldsymbol{\mathcal{L}}^2(\Sigma) \to \widetilde{L^2}(\partial\Omega_\blacksquare)\,, \\ \mathfrak{v} = (v_{ij}, \nu_{ij})_{j<i} &\mapsto \Psi(\mathfrak{v}) = \mathrm{i}\eta \begin{cases} (\nu_{i\blacksquare}, 0) & i = 0, \dots, N \\ (0,0) & 0 \le j < i \le N \end{cases}. \end{aligned}$$

Making use of the fact that by definition of the traces in the beginning of Sect. 2.1 we have $\gamma_D^i = \gamma_D^{\blacksquare,c}$ on $\Gamma_{i\blacksquare}$, $i \in \{0, 1, \dots, N\}$, the following identity holds true:

$$\begin{aligned} &\left\langle\!\left\langle \mathsf{M}_\Sigma(\gamma^\Sigma U - \mathfrak{u}^0_{\mathrm{inc}}), \mathcal{J} \circ \Psi(\mathfrak{v}) \right\rangle\!\right\rangle \\ &\quad = \mathrm{i}\eta \sum_{0\le i\le N} \int_{\Gamma_{i\blacksquare}} \gamma_D^i\, \mathbb{M}_\Sigma(\gamma^\Sigma U - \mathfrak{u}^0_{\mathrm{inc}})\nu_{i\blacksquare}\, \mathrm{d}S \\ &\quad = \mathrm{i}\eta \sum_{0\le i\le N} \int_{\Gamma_{i\blacksquare}} \gamma_D^{\blacksquare,c}\, \mathbb{M}_\Sigma(\gamma^\Sigma U - \mathfrak{u}^0_{\mathrm{inc}})\nu_{i\blacksquare}\, \mathrm{d}S \overset{(4.5)}{=} 0\,, \end{aligned} \tag{4.6}$$

using the straightforward extension of the isometry $\mathcal{J}$ defined in (3.9) to the space

$$\left(\prod_{0\le j<i\le N} L^2(\Gamma_{ij}) \times L^2(\Gamma_{ij})\right) \times \left(\prod_{0\le i\le N} L^2(\Gamma_{i\blacksquare}) \times L^2(\Gamma_{i\blacksquare})\right).$$

Since equation (4.6) holds true for any solution U of (1.2), the following formulation is still consistent with the original problem (1.2).

Formulation 4.1 *Search $\mathfrak{u} \in \boldsymbol{\mathcal{L}}^2(\Sigma)$ such that for all $\mathfrak{v} \in \boldsymbol{\mathcal{L}}^2(\Sigma)$ it holds*

$$\left\langle\!\left\langle (\mathsf{Id} - \mathsf{M}_\Sigma)\mathcal{I}(\mathfrak{u}), \mathcal{J}\,(\mathfrak{v} + \Psi(\mathfrak{v})) \right\rangle\!\right\rangle = \left\langle\!\left\langle \mathfrak{u}_{\mathrm{inc}}, \mathcal{J}\,(\mathfrak{v} + \Psi(\mathfrak{v})) \right\rangle\!\right\rangle. \tag{4.7}$$

Also in this case, uniqueness of solutions is still open (see Remark 3.1).

5 Implementation of the Second-Kind Formulation

5.1 Galerkin Formulation

In this section, we take a closer look at Formulation 3.3, in order to get an idea on how to implement the formulation. For the sake of lucidity, we restrict ourselves to the situation depicted in Fig. 5.1. This situation is sufficiently general to convey all key considerations. The main idea is to consider the trace space on the skeleton Σ interface-wise, as it has already been done in the definition of the L^2 single-trace space (see Def. 3.3) and the L^2 skeleton space (see Def. 3.5). Underlying Definition 3.3 of the single-trace space and the isometry given in (3.8) is the convention that at transmission interfaces the orientation chosen for the interface Γ_{ij} corresponds to the orientation of the adjacent domain Ω_i with larger index $i > j$. The intrinsic orientation is therefore represented by the normal pointing outwards of the domain Ω_i. In the case of $\Gamma_{i\blacksquare}$, if the interface is part of the impenetrable object, we take the

orientation relative to the penetrable domain Ω_i, $i \in \{0, 1, \ldots, N\}$. In Figure 5.1 the intrinsic orientations of the interfaces Γ_{01}, $\Gamma_{0\blacksquare}$ and $\Gamma_{1\blacksquare}$ is indicated through $\mathbf{n}_{01}$, $\mathbf{n}_{0\blacksquare}$ and $\mathbf{n}_{1\blacksquare}$, respectively.

Remark 5.1 (Intrinsic Orientation of Interfaces) *As we will finally conclude, the operators occuring in our formulation can be constructed by* merely using an intrinsic orientation of the interfaces*, no matter how we choose this intrinsic orientation in the beginning. The only additional knowledge we need is the orientation of the adjacent domains with respect to the intrinsic orientation of the interface. There is just one single step where the orientation with respect to adjacent domains matters, namely in the subtraction of the kernels corresponding to two adjacent domains: the kernel of the domain having the orientation opposite to the interface will be subtracted from the kernel associated with the other adjacent domain. In the case of an interface being part of the impenetrable domain, this convention still holds true. We just take "0" as the kernel contribution associated with the impenetrable domain.*

The only reason to introduce the above convention is to simplify the presentation. △

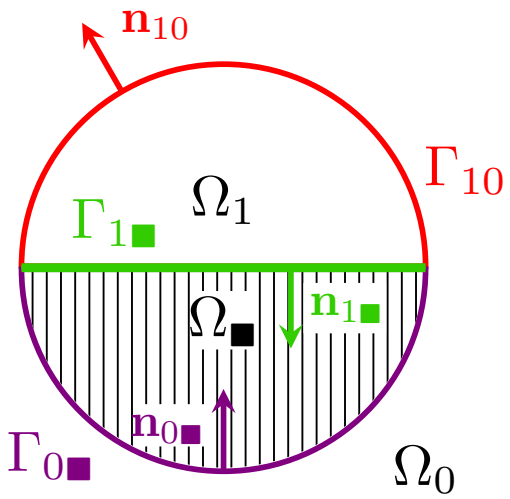

Fig. 5.1: Geometry for structural studies of the second-kind formulation ($N = 1$).

Based on this convention, we study the structure of Formulation 3.3:
Search $\mathfrak{u} \in \boldsymbol{\mathcal{L}}^2(\Sigma)$:

$$\langle\!\langle (\mathsf{Id} - \mathbf{M}_\Sigma)\mathcal{I}(\mathfrak{u}), \mathcal{J}(\mathfrak{v})\rangle\!\rangle = \langle\!\langle \mathfrak{u}_{\text{inc}}, \mathcal{J}(\mathfrak{v})\rangle\!\rangle, \ \forall \mathfrak{v} \in \boldsymbol{\mathcal{L}}^2(\Sigma). \tag{5.1}$$

To begin with, we only consider the second term of the left hand side in (5.1) and we take $\mathfrak{u} = (u_{ij}, \nu_{ij})_{0\le j<i\le N} \in \boldsymbol{\mathcal{L}}^2(\Sigma)$ and $\mathfrak{v} = (v_{ij}, \varphi_{ij})_{0\le j<i\le N} \in$

$\boldsymbol{\mathcal{L}}^2(\Sigma)$. In a first step, we write the test space interface-wise by using the definition of the inner product in (2.10). We also apply the result from Theorem 3.1. It states that if we restrict the definition space of $\mathbf{M}_\Sigma$ to $\boldsymbol{\mathcal{SL}}^2(\Sigma)$, then $\mathrm{Range}(\mathbf{M}_\Sigma) \subset \boldsymbol{\mathcal{SL}}^2(\Sigma)$.

$$\langle\!\langle \mathbf{M}_\Sigma \mathcal{I}(\mathfrak{u}), \mathcal{J}(\mathfrak{v}) \rangle\!\rangle = 2 \sum_{0\le j<i\le N} \int_{\Gamma_{ij}} \gamma_D^i \mathbb{M}_\Sigma(\mathcal{I}(\mathfrak{u}))v_{ij} - \gamma_N^i \mathbb{M}_\Sigma(\mathcal{I}(\mathfrak{u}))\,(-\varphi_{ij})\,\mathrm{d}S + \sum_{0\le i\le N} \int_{\Gamma_{i\blacksquare}} 0 - \gamma_N^i \mathbb{M}_\Sigma(\mathcal{I}(\mathfrak{u}))\,(-\varphi_{ij})\,\mathrm{d}S$$

If we translate this to our concrete example for ($N = 1$) depicted in Fig. 5.1, we get

$$\begin{aligned}&\langle\!\langle \mathbf{M}_\Sigma \mathcal{I}(\mathfrak{u}), \mathcal{J}(\mathfrak{v}) \rangle\!\rangle \\ &\quad= 2\int_{\Gamma_{10}} \gamma_D^1 \mathbb{M}_\Sigma(\mathcal{I}(\mathfrak{u}))v_{10} + \gamma_N^1 \mathbb{M}_\Sigma(\mathcal{I}(\mathfrak{u}))\varphi_{10}\,\mathrm{d}S \\ &\qquad+ \int_{\Gamma_{0\blacksquare}} \gamma_N^0 \mathbb{M}_\Sigma(\mathcal{I}(\mathfrak{u}))\varphi_{0\blacksquare}\,\mathrm{d}S + \int_{\Gamma_{1\blacksquare}} \gamma_N^1 \mathbb{M}_\Sigma(\mathcal{I}(\mathfrak{u}))\varphi_{1\blacksquare}\,\mathrm{d}S\,,\end{aligned}$$

where the colors indicate to which interface a term contributes (see Fig. 5.1). The color red denotes the interface Γ_{10}, violet stands for $\Gamma_{0\blacksquare}$ and green represents $\Gamma_{1\blacksquare}$.

In a next step, we partition the trial space into interface contributions. Hereby, we take into account that at the transmission interface Γ_{10}, we have two adjacent domains contributing to the potential, while for the Dirichlet interfaces $\Gamma_{0\blacksquare}$ and $\Gamma_{1\blacksquare}$, we only have contributions from one side (by our convention from the adjacent domain for which the outward pointing normal coincides with the intrinsic orientation of the interface). Here we interpret the interface-wise defined functions u_{ij}, v_{ij} and ν_{ij}, φ_{ij}, $i,j \in \{\blacksquare, 0, 1, \dots, N\}$ as functions on the whole skeleton Σ by their extension by 0. Nine terms result from splitting trial and test functions into three interface contributions each.

$$\begin{aligned}&\langle\!\langle \mathbf{M}_\Sigma \mathcal{I}(\mathfrak{u}), \mathcal{J}(\mathfrak{v}) \rangle\!\rangle \\ &= 2\int_{\Gamma_{10}} \gamma_D^1(\mathbb{G}_1[\kappa_1])(u_{10},\nu_{10})v_{10} + \gamma_D^1(\mathbb{G}_0[\kappa_0])(u_{10},-\nu_{10})v_{10} \\ &\qquad+\gamma_N^1(\mathbb{G}_1[\kappa_1])(u_{10},\nu_{10})\varphi_{10} + \gamma_N^1(\mathbb{G}_0[\kappa_0])(u_{10},-\nu_{10})\varphi_{10}\,\mathrm{d}S \\ &\quad+2\int_{\Gamma_{10}} \gamma_D^1(\mathbb{G}_0[\kappa_0])(0,\nu_{0\blacksquare})v_{10}\,\mathrm{d}S + 2\int_{\Gamma_{10}} \gamma_D^1(\mathbb{G}_1[\kappa_1])(0,\nu_{1\blacksquare})v_{10}\,\mathrm{d}S \\ &\quad+2\int_{\Gamma_{10}} \gamma_N^1(\mathbb{G}_0[\kappa_0])(0,\nu_{0\blacksquare})\varphi_{10}\,\mathrm{d}S + 2\int_{\Gamma_{10}} \gamma_N^1(\mathbb{G}_1[\kappa_1])(0,\nu_{1\blacksquare})\varphi_{10}\,\mathrm{d}S \\ &\quad+\int_{\Gamma_{0\blacksquare}} \gamma_N^0(\mathbb{G}_1[\kappa_1])(u_{10},\nu_{10})\varphi_{0\blacksquare} + \gamma_N^0(\mathbb{G}_0[\kappa_0])(u_{10},-\nu_{10})\varphi_{0\blacksquare}\,\mathrm{d}S\end{aligned}$$

$$
\begin{aligned}
&+ \int_{\Gamma_{0\blacksquare}} \gamma_N^0(\mathbb{G}_0[\kappa_0])(0,\nu_{0\blacksquare})\varphi_{0\blacksquare} + \gamma_N^0(\mathbb{G}_1[\kappa_1])(0,\nu_{1\blacksquare})\varphi_{0\blacksquare}\,\mathrm{d}S \\
&+ \int_{\Gamma_{1\blacksquare}} \gamma_N^1(\mathbb{G}_1[\kappa_1])(u_{10},\nu_{10})\varphi_{1\blacksquare} + \gamma_N^1(\mathbb{G}_0[\kappa_0])(u_{10},-\nu_{10})\varphi_{1\blacksquare}\,\mathrm{d}S \\
&+ \int_{\Gamma_{1\blacksquare}} \gamma_N^1(\mathbb{G}_0[\kappa_0])(0,\nu_{0\blacksquare})\varphi_{1\blacksquare} + \gamma_N^1(\mathbb{G}_1[\kappa_1])(0,\nu_{1\blacksquare})\varphi_{1\blacksquare}\,\mathrm{d}S
\end{aligned}
$$

In a next step, at the transmission interface Γ_{10} we rewrite the potential that is related to Ω_0, the subdomain that has opposite orientation compared to the intrinsic orientation of Γ_{10}. By definition of the normal $\mathbf{n}_1 = -\mathbf{n}_0$, we have that

$$
\mathbb{G}_0[\kappa_0](u_{10},\nu_{10}) = -\mathbb{G}_1[\kappa_0](u_{10},-\nu_{10}),
$$

and therefore observe

$$
\begin{aligned}
&\langle\!\langle \mathbf{M}_\Sigma \mathcal{I}(\mathbf{u}), \mathcal{J}(\mathbf{v})\rangle\!\rangle \\
&= 2\int_{\Gamma_{10}} \gamma_D^1(\mathbb{G}_1[\kappa_1] - \mathbb{G}_1[\kappa_0])(u_{10},\nu_{10})v_{10} \\
&\qquad + \gamma_N^1(\mathbb{G}_1[\kappa_1] - \mathbb{G}_1[\kappa_0])(u_{10},\nu_{10})\varphi_{10}\,\mathrm{d}S \\
&\quad + 2\int_{\Gamma_{10}} \gamma_D^1(\mathbb{G}_0[\kappa_0])(0,\nu_{0\blacksquare})v_{10}\,\mathrm{d}S + 2\int_{\Gamma_{10}} \gamma_D^1(\mathbb{G}_1[\kappa_1])(0,\nu_{1\blacksquare})v_{10}\,\mathrm{d}S \\
&\quad + 2\int_{\Gamma_{10}} \gamma_N^1(\mathbb{G}_0[\kappa_0])(0,\nu_{0\blacksquare})\varphi_{10}\,\mathrm{d}S + 2\int_{\Gamma_{10}} \gamma_N^1(\mathbb{G}_1[\kappa_1])(0,\nu_{1\blacksquare})\varphi_{10}\,\mathrm{d}S \\
&\quad + \int_{\Gamma_{0\blacksquare}} \gamma_N^0(\mathbb{G}_1[\kappa_1] - \mathbb{G}_1[\kappa_0])(u_{10},\nu_{10})\varphi_{0\blacksquare}\,\mathrm{d}S \\
&\quad + \int_{\Gamma_{0\blacksquare}} \gamma_N^0(\mathbb{G}_0[\kappa_0])(0,\nu_{0\blacksquare})\varphi_{0\blacksquare} + \gamma_N^0(\mathbb{G}_1[\kappa_1])(0,\nu_{1\blacksquare})\varphi_{0\blacksquare}\,\mathrm{d}S \\
&\quad + \int_{\Gamma_{1\blacksquare}} \gamma_N^1(\mathbb{G}_1[\kappa_1] - \mathbb{G}_1[\kappa_0])(u_{10},\nu_{10})\varphi_{1\blacksquare}\,\mathrm{d}S \\
&\quad + \int_{\Gamma_{1\blacksquare}} \gamma_N^1(\mathbb{G}_0[\kappa_0])(0,\nu_{0\blacksquare})\varphi_{1\blacksquare} + \gamma_N^1(\mathbb{G}_1[\kappa_1])(0,\nu_{1\blacksquare})\varphi_{1\blacksquare}\,\mathrm{d}S
\end{aligned}
$$

Finally, we have derived an interface-wise representation of Formulation 3.3. Assuming that we are working in a finite dimensional space $V_M \subset \boldsymbol{\mathcal{L}}^2(\Sigma)$ of dimension M, we can represent our test and trial functions restricted to each interface Γ_{ij} as linear combinations with respect to a local basis $\{b_{ij}^1, \ldots, b_{ij}^{M_{ij}}\}$. For instance

$$
u_{10}(\boldsymbol{x}) = \sum_{i=1}^{M_{10}} u_{10}^i b_{10}^i(\boldsymbol{x}),\ \vec{\mathbf{u}}_{10} \coloneqq \begin{pmatrix} u_{10}^1 & \ldots & u_{10}^{M_{10}} \end{pmatrix}^\top,\ \boldsymbol{x} \in \Gamma_{10}\,. \tag{5.2}
$$

Writing the contributions in block form leads to the following block partitioned system matrix. We will first state the matrix and then explain how the matrix blocks look like

$$\begin{pmatrix} \mathbf{C}_{10}^{10} & \mathbf{C}_{0\blacksquare}^{10} & \mathbf{C}_{1\blacksquare}^{10} \\ \mathbf{C}_{10}^{0\blacksquare} & \mathbf{C}_{0\blacksquare}^{0\blacksquare} & \mathbf{C}_{1\blacksquare}^{0\blacksquare} \\ \mathbf{C}_{10}^{1\blacksquare} & \mathbf{C}_{0\blacksquare}^{1\blacksquare} & \mathbf{C}_{1\blacksquare}^{1\blacksquare} \end{pmatrix} \in \mathbb{C}^{M,M}\,, \quad M := 2M_{10} + M_{0\blacksquare} + M_{1\blacksquare}\,, \tag{5.3}$$

with

$$\mathbf{C}_{10}^{10} := 2\begin{pmatrix} -\left(\mathbf{K}_{10}^{10}[\kappa_1] - \mathbf{K}_{10}^{10}[\kappa_0]\right) & \mathbf{V}_{10}^{10}[\kappa_1] - \mathbf{V}_{10}^{10}[\kappa_0] \\ \mathbf{W}_{10}^{10}[\kappa_1] - \mathbf{W}_{10}^{10}[\kappa_0] & \mathbf{K}'^{10}_{10}[\kappa_1] - \mathbf{K}'^{10}_{10}[\kappa_0] \end{pmatrix},$$

the difference of two "Calderón operators" (see [33, equation (3.122)]), where

$$\mathbf{K}_{10}^{10}[\kappa_1] - \mathbf{K}_{10}^{10}[\kappa_0] := \Big(\int_{\Gamma_{10}} \gamma_D^1(\mathbb{D}_1[\kappa_1] - \mathbb{D}_1[\kappa_0])(b_{10}^j) b_{10}^i \,\mathrm{d}S \Big)_{i,j=1}^{M_{10}} \in \mathbb{C}^{M_{10},M_{10}}$$

represents the difference of two double layer operators (see [33, Sect. 3.3.3]). The difference of two single layer operators (c.f. [33, 3.3.2]) gives rise to the matrix

$$\mathbf{V}_{10}^{10}[\kappa_1] - \mathbf{V}_{10}^{10}[\kappa_0] := \Big(\int_{\Gamma_{10}} \gamma_D^1(\mathbb{S}_1[\kappa_1] - \mathbb{S}_1[\kappa_0])(b_{10}^j) b_{10}^i \,\mathrm{d}S \Big)_{i,j=1}^{M_{10}} \in \mathbb{C}^{M_{10},M_{10}}$$

and the difference of two hypersingular operators (c.f. [33, Sect. 3.3.4]) and two adjoint double layer operators (see [33, Sect. 3.3.3]), respectively, leads to the matrices

$$\mathbf{W}_{10}^{10}[\kappa_1] - \mathbf{W}_{10}^{10}[\kappa_0] := \Big(-\int_{\Gamma_{10}} \gamma_N^1(\mathbb{D}_1[\kappa_1] - \mathbb{D}_1[\kappa_0])(b_{10}^j) b_{10}^i \,\mathrm{d}S \Big)_{i,j=1}^{M_{10}}, \tag{5.4}$$

and

$$\mathbf{K}'^{10}_{10}[\kappa_1] - \mathbf{K}'^{10}_{10}[\kappa_0] := \Big(\int_{\Gamma_{10}} \gamma_N^1(\mathbb{S}_1[\kappa_1] - \mathbb{S}_1[\kappa_0])(b_{10}^j) b_{10}^i \,\mathrm{d}S \Big)_{i,j=1}^{M_{10}} \in \mathbb{C}^{M_{10},M_{10}}.$$

Obviously, at transmission interfaces we obtain differences of the classical kernels. The operators associated with transmission interfaces are studied in great detail in [11, Lem. 5.3]. Taking the difference of two kernels leads to cancellation of leading singularities such that the integrals given in $\mathbf{C}_{10}^{10}$ are at most weakly singular. This makes it easier to treat the operators numerically. On the other hand, it is important to emphasise that numerical cancellation becomes a key issue in the implementation (see [11, p.51/52]). Therefore, one should implement an extra kernel for subtracted operators and treat it in such a way that numerical cancellation is reduced to a minimum. In our implementation, we use Taylor expansions to achieve a numerically stable implementation (see [11, eq. (5.7)-(5.9)]).

The next block is a coupling term of the Dirichlet interface $\Gamma_{0\blacksquare}$ and the transmission interface Γ_{10}:

$$\mathbf{C}^{10}_{0\blacksquare} := 2\begin{pmatrix}\left(\int_{\Gamma_{10}} \gamma^1_D(\mathbb{S}_0[\kappa_0])(b^j_{0\blacksquare})b^i_{10}\,\mathrm{d}S\right)_{\substack{1\le i\le M_{10}\\1\le j\le M_{0\blacksquare}}}\\ \left(\int_{\Gamma_{10}} \gamma^1_N(\mathbb{S}_0[\kappa_0])(b^j_{0\blacksquare})b^i_{10}\,\mathrm{d}S\right)_{\substack{1\le i\le M_{10}\\1\le j\le M_{0\blacksquare}}}\end{pmatrix} = \begin{pmatrix}\mathbf{V}^{10}_{0\blacksquare}[\kappa_0]\\ \mathbf{K}'^{10}_{0\blacksquare}[\kappa_0]\end{pmatrix}.$$

In this case no cancellation occurs, since at the Dirichlet boundary we only have a potential contribution from one side. Therefore, we need to treat kernels of the types $\gamma^1_D(\mathbb{S}_1[\kappa_1])$, $\gamma^1_N(\mathbb{S}_1[\kappa_1])$ (see for instance $\mathbf{C}^{10}_{0\blacksquare}$). The first kernel corresponds to the weakly singular operator $\mathbf{V}^{10}_{0\blacksquare}$ and is weakly singular, while the second term, i.e. the kernel of the adjoint double layer operator $\mathbf{K}'^{10}_{0\blacksquare}$, has a strong singularity behaving like $\mathcal{O}(\frac{1}{\|\boldsymbol{x}-\boldsymbol{y}\|})$ for $d=2$ and $\mathcal{O}(\frac{1}{\|\boldsymbol{x}-\boldsymbol{y}\|^2})$ for $d=3$, respectively. Therefore, we face a principal part integral, which finally leads to a "jump term" $\frac{1}{2}\mathsf{Id}$, when crossing the interface $\Gamma_{0\blacksquare}$ (see [26, Sec. 7.2]). In the case of $\mathbf{C}^{10}_{0\blacksquare}$, we can neglect this term because our trial space is restricted to the interface Γ_{10}.

The same applies to the third block in the first row.

$$\mathbf{C}^{10}_{1\blacksquare} := 2\begin{pmatrix}\left(\int_{\Gamma_{10}} \gamma^1_D(\mathbb{S}_1[\kappa_1])(b^j_{1\blacksquare})b^i_{10}\,\mathrm{d}S\right)_{\substack{1\le i\le M_{10}\\1\le j\le M_{1\blacksquare}}}\\ \left(\int_{\Gamma_{10}} \gamma^1_N(\mathbb{S}_1[\kappa_1])(b^j_{1\blacksquare})b^i_{10}\,\mathrm{d}S\right)_{\substack{1\le i\le M_{10}\\1\le j\le M_{1\blacksquare}}}\end{pmatrix} = \begin{pmatrix}\mathbf{V}^{10}_{0\blacksquare}[\kappa_0]\\ \mathbf{K}'^{10}_{0\blacksquare}[\kappa_0]\end{pmatrix}.$$

The blocks in the second row of (5.3) correspond to test functions associated with $\Gamma_{0\blacksquare}$. Since the first block $\mathbf{C}^{0\blacksquare}_{10}$ is associated with the trial functions supported on the transmission interface Γ_{10}, we again obtain less singular differences of classical kernels, which feature at most weak singularities.

$$\begin{aligned}\mathbf{C}^{0\blacksquare}_{10} &:= \begin{pmatrix}\left(-\int_{\Gamma_{0\blacksquare}} \gamma^0_N(\mathbb{D}_1[\kappa_1]-\mathbb{D}_1[\kappa_0])(b^j_{10})b^i_{0\blacksquare}\,\mathrm{d}S\right)_{\substack{1\le i\le M_{0\blacksquare}\\1\le j\le M_{10}}}\\ \left(\int_{\Gamma_{0\blacksquare}} \gamma^0_N(\mathbb{S}_1[\kappa_1]-\mathbb{S}_1[\kappa_0])(b^j_{10})b^i_{0\blacksquare}\,\mathrm{d}S\right)_{\substack{1\le i\le M_{0\blacksquare}\\1\le j\le M_{10}}}\end{pmatrix}^{\mathsf{T}}\\ &= \left(\mathbf{W}^{0\blacksquare}_{10}[\kappa_1]-\mathbf{W}^{0\blacksquare}_{10}[\kappa_0]\;\mathbf{K}'^{0\blacksquare}_{10}[\kappa_1]-\mathbf{K}'^{0\blacksquare}_{10}[\kappa_0]\right).\end{aligned}$$

The second block $\mathbf{C}^{0\blacksquare}_{0\blacksquare}$ in the second row of (5.3) is the self-interaction of $\Gamma_{0\blacksquare}$. As mentioned above, since the kernel $\gamma^0_{N,\boldsymbol{x}}\gamma^0_{D,\boldsymbol{y}}\Phi_{\kappa_0}(\boldsymbol{x},\boldsymbol{y})$ of $\gamma^0_N(\mathbb{S}_0[\kappa_0])$ has a strong singularity in $\boldsymbol{x}=\boldsymbol{y}$, we obtain a contribution $\frac{1}{2}\mathsf{Id}$ due to the principal part integral when crossing the interface $\Gamma_{0\blacksquare}$. After Galerkin discretisation, this jump term is represented by

$$\frac{1}{2}\mathbf{M}^{0\blacksquare}_{0\blacksquare} = \frac{1}{2}\left(\int_{\Gamma_{0\blacksquare}} b^j_{0\blacksquare}b^i_{0\blacksquare}\,\mathrm{d}S\right)^{M_{0\blacksquare}}_{i,j=1}.$$

Thus, we obtain

$$\mathbf{C}^{0\blacksquare}_{0\blacksquare} := \left(\int_{\Gamma_{0\blacksquare}} \gamma^0_N(\mathbb{S}_0[\kappa_0])(b^j_{0\blacksquare})b^i_{0\blacksquare}\,\mathrm{d}S\right)^{M_{0\blacksquare}}_{i,j=1} = \frac{1}{2}\mathbf{M}^{0\blacksquare}_{0\blacksquare} + \mathbf{K}'^{0\blacksquare}_{0\blacksquare}[\kappa_0],$$

as in the case of the second-kind formulation of the exterior Dirichlet problem.

The last block $\mathbf{C}^{0\blacksquare}_{1\blacksquare}$ in the second row has the form

$$\mathbf{C}^{0\blacksquare}_{1\blacksquare} := \Big(\int_{\Gamma_{0\blacksquare}} \gamma^0_N(\mathbb{S}_1[\kappa_1])(b^j_{1\blacksquare}) b^i_{0\blacksquare} \,\mathrm{d}S \Big)_{\substack{1\le i\le M_{0\blacksquare} \\ 1\le j\le M_{1\blacksquare}}} = \mathbf{K'}^{0\blacksquare}_{1\blacksquare}[\kappa_1] \,.$$

Finally, the last row of the block matrix in (5.3) can be obtained analogously to the second row blocks.

$$\begin{aligned}
\mathbf{C}^{1\blacksquare}_{10} &:= \begin{pmatrix} \Big(-\int_{\Gamma_{1\blacksquare}} \gamma^1_N(\mathbb{D}_1[\kappa_1] - \mathbb{D}_1[\kappa_0])(b^j_{10}) b^i_{1\blacksquare} \,\mathrm{d}S \Big)_{\substack{1\le i\le M_{1\blacksquare} \\ 1\le j\le M_{10}}} \\ \Big(\int_{\Gamma_{0\blacksquare}} \gamma^1_N(\mathbb{S}_1[\kappa_1] - \mathbb{S}_1[\kappa_0])(b^j_{10}) b^i_{1\blacksquare} \,\mathrm{d}S \Big)_{\substack{1\le i\le M_{1\blacksquare} \\ 1\le j\le M_{10}}} \end{pmatrix}^\top \\
&= \big(\mathbf{W}^{1\blacksquare}_{10}[\kappa_1] - \mathbf{W}^{1\blacksquare}_{10}[\kappa_0] \;\; \mathbf{K'}^{1\blacksquare}_{10}[\kappa_1] - \mathbf{K'}^{1\blacksquare}_{10}[\kappa_0] \big) \,, \\
\mathbf{C}^{1\blacksquare}_{0\blacksquare} &:= \Big(\int_{\Gamma_{1\blacksquare}} \gamma^1_N(\mathbb{S}_0[\kappa_0])(b^j_{0\blacksquare}) b^i_{1\blacksquare} \,\mathrm{d}S \Big)_{\substack{1\le i\le M_{1\blacksquare} \\ 1\le j\le M_{0\blacksquare}}} = \mathbf{K'}^{1\blacksquare}_{0\blacksquare}[\kappa_0] \,, \\
\mathbf{C}^{1\blacksquare}_{1\blacksquare} &:= \Big(\int_{\Gamma_{0\blacksquare}} \gamma^1_N(\mathbb{S}_1[\kappa_1])(b^j_{1\blacksquare}) b^i_{0\blacksquare} \,\mathrm{d}S \Big)^{M_{0\blacksquare}}_{i,j=1} = \frac{1}{2}\mathbf{M}^{1\blacksquare}_{1\blacksquare} + \mathbf{K'}^{1\blacksquare}_{1\blacksquare}[\kappa_1] \,.
\end{aligned}$$

Using the interface-wise decomposition in (5.3), we finally observe the following block structure for the linear system of equations arising from the Galerkin discretisation of Formulaiton 3.3 in the case of the geometry depicted in Figure 5.1 and restricting to a finite dimensional subspace $V_M \subset \boldsymbol{\mathcal{L}}^2(\Sigma)$.

Linear System of Equations 5.1
Find $\vec{\mathbf{u}} = (\vec{\mathbf{u}}_{10}, \vec{\boldsymbol{\varphi}}_{10}, \vec{\boldsymbol{\varphi}}_{0,\blacksquare}, \vec{\boldsymbol{\varphi}}_{1,\blacksquare})^\top \in \mathbb{C}^{2M_{10}+M_{0\blacksquare}+M_{1\blacksquare}}$, *such that*

$$\begin{aligned}
&\left(\begin{pmatrix} 2\mathbf{M}^{10}_{10} & \mathbf{0} & \mathbf{0} & \mathbf{0} \\ \mathbf{0} & 2\mathbf{M}^{10}_{10} & \mathbf{0} & \mathbf{0} \\ \mathbf{0} & \mathbf{0} & \frac{1}{2}\mathbf{M}^{0\blacksquare}_{0\blacksquare} & \mathbf{0} \\ \mathbf{0} & \mathbf{0} & \mathbf{0} & \frac{1}{2}\mathbf{M}^{1\blacksquare}_{1\blacksquare} \end{pmatrix} \right. \\
&\quad \left. - \begin{pmatrix} -2(\mathbf{K}^{10}_{10}[\kappa_1] - \mathbf{K}^{10}_{10}[\kappa_0]) & 2(\mathbf{V}^{10}_{10}[\kappa_1] - \mathbf{V}^{10}_{10}[\kappa_0]) & 2\mathbf{V}^{10}_{0\blacksquare}[\kappa_0] & 2\mathbf{V}^{10}_{1\blacksquare}[\kappa_0] \\ 2(\mathbf{W}^{10}_{10}[\kappa_1] - \mathbf{W}^{10}_{10}[\kappa_0]) & 2(\mathbf{K'}^{10}_{10}[\kappa_1] - \mathbf{K'}^{10}_{10}[\kappa_0]) & 2\mathbf{K'}^{10}_{0\blacksquare}[\kappa_0] & 2\mathbf{K'}^{10}_{1\blacksquare}[\kappa_0] \\ \mathbf{W}^{0\blacksquare}_{10}[\kappa_1] - \mathbf{W}^{0\blacksquare}_{10}[\kappa_0] & \mathbf{K'}^{0\blacksquare}_{10}[\kappa_1] - \mathbf{K'}^{0\blacksquare}_{10}[\kappa_0] & \mathbf{K'}^{0\blacksquare}_{0\blacksquare}[\kappa_0] & \mathbf{K'}^{0\blacksquare}_{1\blacksquare}[\kappa_1] \\ \mathbf{W}^{1\blacksquare}_{10}[\kappa_1] - \mathbf{W}^{1\blacksquare}_{10}[\kappa_0] & \mathbf{K'}^{1\blacksquare}_{10}[\kappa_1] - \mathbf{K'}^{1\blacksquare}_{10}[\kappa_0] & \mathbf{K'}^{1\blacksquare}_{0\blacksquare}[\kappa_0] & \mathbf{K'}^{1\blacksquare}_{1\blacksquare}[\kappa_1] \end{pmatrix} \right) \begin{pmatrix} \vec{\mathbf{u}}_{10} \\ \vec{\boldsymbol{\varphi}}_{10} \\ \vec{\boldsymbol{\varphi}}_{0\blacksquare} \\ \vec{\boldsymbol{\varphi}}_{1\blacksquare} \end{pmatrix} \\
&\qquad = \begin{pmatrix} 2\mathbf{M}^{10}_{10} & \mathbf{0} & \mathbf{0} & \mathbf{0} \\ \mathbf{0} & 2\mathbf{M}^{10}_{10} & \mathbf{0} & \mathbf{0} \\ \mathbf{0} & \mathbf{0} & \mathbf{M}^{0\blacksquare}_{0\blacksquare} & \mathbf{0} \\ \mathbf{0} & \mathbf{0} & \mathbf{0} & \mathbf{M}^{1\blacksquare}_{1\blacksquare} \end{pmatrix} \begin{pmatrix} \overrightarrow{\boldsymbol{\gamma}^1_{\mathbf{D}} \mathbf{U}_{\mathbf{inc}10}} \\ \overrightarrow{\boldsymbol{\gamma}^1_{\mathbf{N}} \mathbf{U}_{\mathbf{inc}10}} \\ \overrightarrow{\boldsymbol{\gamma}^0_{\mathbf{N}} \mathbf{U}_{\mathbf{inc}0\blacksquare}} \\ \overrightarrow{\boldsymbol{\gamma}^1_{\mathbf{N}} \mathbf{U}_{\mathbf{inc}1\blacksquare}} \end{pmatrix},
\end{aligned}$$

where $\overrightarrow{\boldsymbol{\gamma}^{\mathbf{i}}_{\mathbf{N}} \mathbf{U}_{\mathbf{inc}ij}}$ *and* $\overrightarrow{\boldsymbol{\gamma}^{\mathbf{i}}_{\mathbf{D}} \mathbf{U}_{\mathbf{inc}ij}}$ *represent coefficient vectors of the interpolant of* U_{inc} *in the finite dimensional space* $V_M \subset \boldsymbol{\mathcal{L}}^2(\Sigma)$, *restricted to the interface* Γ_{ij}, $i,j \in \{\blacksquare, 0, 1\}$.

The Linear System of Equations 5.1, arising from Galerkin discretisation in the setting of Fig. 5.1, is rather typical. For other geometries the structure is exactly the same: when both spaces, i.e. test and trial space, are associated with a transmission interface, then matrices of the form

$$2\begin{pmatrix} \mathbf{M}_{10}^{10} & \mathbf{0} \\ \mathbf{0} & \mathbf{M}_{10}^{10} \end{pmatrix} - \mathbf{C}_{10}^{10}$$

occur. The mass term is dropped in the case of two different transmission interfaces. If we consider a block where both spaces are associated with Dirichlet interfaces, then the matrices are of the form $\mathbf{M}_{1\blacksquare}^{1\blacksquare} - \mathbf{C}_{1\blacksquare}^{1\blacksquare}[\kappa_1]$ in the case of a self-coupling and of the form $\mathbf{C}_{1\blacksquare}^{0\blacksquare}$ in every other case. The coupling blocks have the form $\mathbf{C}_{0\blacksquare}^{10}[\kappa_0]$, if the test space is associated with a Dirichlet interface and the trial space with a transmission interface, vice versa for $\mathbf{C}_{10}^{0\blacksquare}[\kappa_0]$.

5.2 Galerkin Formulation for CFIE Formulation 4.1

As in the previous subsection, we will consider the geometry depicted in Figure 5.1. Let $\boldsymbol{G}$ be the matrix on the left hand side of the Linear System of Equations 5.1. Then, we observe that the Galerkin matrix $\boldsymbol{G}_{\mathrm{CFIE}}$ corresponding to Formulation 4.1 has the following form:

$$\boldsymbol{G}_{\mathrm{CFIE}} \coloneqq \boldsymbol{G} + i\eta \begin{pmatrix} \mathbf{0} & \mathbf{0} & \mathbf{0} & \mathbf{0} \\ \mathbf{0} & \mathbf{0} & \mathbf{0} & \mathbf{0} \\ -(\mathbf{K}_{10}^{0\blacksquare}[\kappa_1] - \mathbf{K}_{10}^{0\blacksquare}[\kappa_0]) & \mathbf{V}_{10}^{0\blacksquare}[\kappa_1] - \mathbf{V}_{10}^{0\blacksquare}[\kappa_0] & \mathbf{V}_{0\blacksquare}^{0\blacksquare}[\kappa_0] & \mathbf{V}_{1\blacksquare}^{0\blacksquare}[\kappa_1] \\ -(\mathbf{K}_{10}^{1\blacksquare}[\kappa_1] - \mathbf{K}_{10}^{1\blacksquare}[\kappa_0]) & \mathbf{V}_{10}^{1\blacksquare}[\kappa_1] - \mathbf{V}_{10}^{1\blacksquare}[\kappa_0] & \mathbf{V}_{0\blacksquare}^{1\blacksquare}[\kappa_0] & \mathbf{V}_{1\blacksquare}^{1\blacksquare}[\kappa_1] \end{pmatrix}. \quad (5.5)$$

For the right hand side vector we observe

$$\boldsymbol{y}_{\mathrm{CFIE}} \coloneqq \left(\begin{pmatrix} 2\mathbf{M}_{10}^{10} & \mathbf{0} & \mathbf{0} & \mathbf{0} \\ \mathbf{0} & 2\mathbf{M}_{10}^{10} & \mathbf{0} & \mathbf{0} \\ \mathbf{0} & \mathbf{0} & \mathbf{M}_{0\blacksquare}^{0\blacksquare} & \mathbf{0} \\ \mathbf{0} & \mathbf{0} & \mathbf{0} & \mathbf{M}_{1\blacksquare}^{1\blacksquare} \end{pmatrix} + i\eta \begin{pmatrix} 0\,0 & 0 & 0 \\ 0\,0 & 0 & 0 \\ 0\,0 & \mathbf{M}_{0\blacksquare}^{0\blacksquare} & \mathbf{0} \\ 0\,0 & \mathbf{0} & \mathbf{M}_{1\blacksquare}^{1\blacksquare} \end{pmatrix} \right) \begin{pmatrix} \overrightarrow{\gamma_{\mathrm{D}}^{1}\,\mathbf{U}_{\mathbf{inc}}}_{10} \\ \overrightarrow{\gamma_{\mathrm{N}}^{1}\,\mathbf{U}_{\mathbf{inc}}}_{10} \\ \overrightarrow{\gamma_{\mathrm{N}}^{0}\,\mathbf{U}_{\mathbf{inc}}}_{0\blacksquare} \\ \overrightarrow{\gamma_{\mathrm{N}}^{1}\,\mathbf{U}_{\mathbf{inc}}}_{1\blacksquare} \end{pmatrix}, \quad (5.6)$$

and therefore obtain the following linear system of equations arising from the Galerkin BEM discretisation of CFIE Formulation 4.1.

Linear System of Equations 5.2
Find $\vec{\mathbf{u}} = (\vec{\mathbf{u}}_{10}, \vec{\boldsymbol{\varphi}}_{10}, \vec{\boldsymbol{\varphi}}_{0,\blacksquare}, \vec{\boldsymbol{\varphi}}_{1,\blacksquare})^{\top} \in \mathbb{C}^{2M_{10}+M_{0\blacksquare}+M_{1\blacksquare}}$, *such that*

$$\boldsymbol{G}_{CFIE} \begin{pmatrix} \vec{\mathbf{u}}_{10} \\ \vec{\boldsymbol{\varphi}}_{10} \\ \vec{\boldsymbol{\varphi}}_{0\blacksquare} \\ \vec{\boldsymbol{\varphi}}_{1\blacksquare} \end{pmatrix} = \boldsymbol{y}_{CFIE},$$

where $\boldsymbol{G}_{CFIE}$ *and* $\boldsymbol{y}_{CFIE}$ *are given in* (5.5) *and* (5.6)*, respectively.*

5.3 Inhomogeneous Dirichlet Boundary Conditions

For non-vanishing Dirichlet boundary conditions on $\partial\Omega_{\blacksquare}$, i.e. $\gamma_D^{\blacksquare} U = \mathfrak{g}$, we assume that $\mathfrak{g} \in H^1(\partial\Omega_{\blacksquare})$. If we consider Formulation 4.1 for non-vanishing Dirichlet boundary conditions in the case of the scatterer depicted in Figure 5.1, we obtain the following right hand side of the Linear System of Equations 5.1:

$$\boldsymbol{y}_D = \begin{pmatrix} 2\mathbf{M}_{10}^{10} & \mathbf{0} & \mathbf{0} & \mathbf{0} \\ \mathbf{0} & 2\mathbf{M}_{10}^{10} & \mathbf{0} & \mathbf{0} \\ \mathbf{0} & \mathbf{0} & \mathbf{M}_{0\blacksquare}^{0\blacksquare} & \mathbf{0} \\ \mathbf{0} & \mathbf{0} & \mathbf{0} & \mathbf{M}_{1\blacksquare}^{1\blacksquare} \end{pmatrix} \begin{pmatrix} \overrightarrow{\gamma_{\mathrm{D}}^{1}\,\mathbf{U}_{\mathrm{inc}\,10}} \\ \overrightarrow{\gamma_{\mathrm{N}}^{1}\,\mathbf{U}_{\mathrm{inc}\,10}} \\ \overrightarrow{\gamma_{\mathrm{N}}^{0}\,\mathbf{U}_{\mathrm{inc}\,0\blacksquare}} \\ \overrightarrow{\gamma_{\mathrm{N}}^{1}\,\mathbf{U}_{\mathrm{inc}\,1\blacksquare}} \end{pmatrix} + \begin{pmatrix} -2\mathbf{K}_{0\blacksquare}^{10} & -2\boldsymbol{K}_{1\blacksquare}^{10} \\ 2\widetilde{\mathbf{W}}_{0\blacksquare}^{10} & 2\widetilde{\mathbf{W}}_{1\blacksquare}^{10} \\ \widetilde{\mathbf{W}}_{0\blacksquare}^{0\blacksquare} & \widetilde{\mathbf{W}}_{1\blacksquare}^{0\blacksquare} \\ \widetilde{\mathbf{W}}_{0\blacksquare}^{1\blacksquare} & \widetilde{\mathbf{W}}_{1\blacksquare}^{1\blacksquare} \end{pmatrix} \begin{pmatrix} \overrightarrow{\mathfrak{g}}_{0\blacksquare} \\ \overrightarrow{\mathfrak{g}}_{1\blacksquare} \end{pmatrix}.$$

It is important to notice, that in this case, we will have contributions of the hypersingular operators $\widetilde{\mathbf{W}}_{i\blacksquare}^{pq}$ (see [33, Sect. 3.3.4]) also at Dirichlet interfaces. Since the operator has a form different from that of the operator $\mathbf{W}_{10}^{10}$, given in (5.4), we tag it with a tilde $\widetilde{\cdot}$. As we learned in Subsection 5.1, at $\partial\Omega_{\blacksquare}$, no cancellation of kernel singularities takes place. This means that in order to obtain a numerically tractable operator, we need to resort to integration by parts. In what follows, an explanation of a regularisation strategy is given.

Since our test space is discontinuous, the classical approach involving integration by parts twice is not applicable (see [33, Sect. 3.3.4] or [34, Sect. 6.5]). Instead, we apply integration by parts only once and use continuous ansatz functions to approximate the Dirichlet data $\mathfrak{g}$ on $\partial\Omega_{\blacksquare}$ (cf. *Maue's Formula* for example in [27, equations (10) and (11)]).

When applying integration by parts, we have to be careful at junction points/intersections, i.e. points/intersections where two or more interfaces abut. There, we will encounter jumps in the wave number and therefore boundary terms will emerge.

Let $\widetilde{b}_{i\blacksquare}^{j}$, $j \in \{1, \dots, M_{i\blacksquare}\}$ denote the restrictions to $\Gamma_{i\blacksquare}$ of the piecewise continuous basis functions of the finite dimensional subspace $\widetilde{V}_M \subset H^1(\partial\Omega_{\blacksquare})$ and let $\left\{b_{pq}^1, \dots, b_{pq}^{M_{pq}}\right\}$ denote the basis of $V_M \subset \boldsymbol{\mathcal{L}}^2(\Sigma)$ restricted to $L^2(\Gamma_{pq})$, $pq \in \{10, 0\blacksquare, 1\blacksquare\}$, $i \in \{0, 1\}$. Then, we get

$$\widetilde{\boldsymbol{W}}_{i\blacksquare}^{pq} := \Big(-\int_{\Gamma_{pq}} \gamma_N^q\, \mathbb{D}_i[\kappa_i](\widetilde{b}_{i\blacksquare}^{j}) b_{pq}^{l}\, \mathrm{d}S\Big)_{\substack{l=1,\dots,M_{pq} \\ j=1,\dots,M_{i\blacksquare}}},$$

and for $\boldsymbol{r} := \boldsymbol{x} - \boldsymbol{y}$, when applying integration by parts (see [34, Proof of Lemma 6.16, Theorem 6.17]), we obtain in the case $d = 3$ that

$$\begin{aligned} \left(\widetilde{\boldsymbol{W}}_{i\blacksquare}^{pq}\right)_{lj} &= -\int_{\Gamma_{pq}} \gamma_N^p\, \mathbb{D}_i[\kappa_i](b_{i\blacksquare}^{j}) b_{pq}^{l}\, \mathrm{d}S \\ &= -\lim_{\epsilon\to 0} \int_{\Gamma_{pq}} \mathbf{n}_p(\boldsymbol{x}) \cdot \mathbf{grad}_{\boldsymbol{x}} \left(\int_{\substack{\boldsymbol{y}\in\Gamma_{i\blacksquare} \\ \|\boldsymbol{x}-\boldsymbol{y}\|\geq\epsilon}} \mathbf{n}_i(\boldsymbol{y}) \cdot \mathbf{grad}_{\boldsymbol{y}}\, \Phi_{\kappa_i}(\boldsymbol{r}) \right. \end{aligned}$$

$$\widetilde{b}^j_{i\blacksquare}(\boldsymbol{y}) b^l_{pq}(\boldsymbol{x}) \mathrm{d}S(\boldsymbol{y}) \Big) \mathrm{d}S(\boldsymbol{x})$$

$$= -\lim_{\epsilon \to 0} \int_{\Gamma_{pq}} \int_{\substack{\boldsymbol{y} \in \Gamma_{i\blacksquare} \\ \|\boldsymbol{x}-\boldsymbol{y}\| \geq \epsilon}} \mathbf{curl}_{\Gamma_{pq},\boldsymbol{x}} \Phi_{\kappa_i}(\boldsymbol{r}) \cdot \mathbf{curl}_{\Gamma_{i\blacksquare},\boldsymbol{y}} (\widetilde{b}^j_{i\blacksquare})(\boldsymbol{y}) b^l_{pq}(\boldsymbol{x}) \mathrm{d}S(\boldsymbol{y}) \mathrm{d}S(\boldsymbol{x})$$

$$- \kappa_i^2 \int_{\Gamma_{pq}} \int_{\Gamma_{i\blacksquare}} \mathbf{n}_i(\boldsymbol{y}) \cdot \mathbf{n}_p(\boldsymbol{x}) \Phi_{\kappa_i}(\boldsymbol{r}) \widetilde{b}^j_{i\blacksquare}(\boldsymbol{y}) b^l_{pq}(\boldsymbol{x}) \mathrm{d}S(\boldsymbol{y}) \mathrm{d}S(\boldsymbol{x})$$

$$- \int_{\Gamma_{pq}} \int_{\partial \Gamma_{i\blacksquare}} \widetilde{b}^l_{i\blacksquare}(\boldsymbol{y}) \, \mathbf{curl}_{\Gamma_{pq},\boldsymbol{x}} \Phi_{\kappa_i}(\boldsymbol{r}) \cdot \mathrm{d}\sigma(\boldsymbol{y}) \mathrm{d}S(\boldsymbol{x}) \,, \tag{5.7}$$

where

$$\mathbf{curl}_{\Gamma_{i\blacksquare},\boldsymbol{y}} v = \mathbf{n}_i(\boldsymbol{y}) \times \mathbf{grad}_{\boldsymbol{y}} V \,, \; \mathbf{curl}_{\Gamma_{pq},\boldsymbol{x}} v = \mathbf{n}_p(\boldsymbol{x}) \times \mathbf{grad}_{\boldsymbol{x}} V \,,$$

denotes the surface curl (see [34, p.133]) and V is a suitable extension of v on $\Gamma_{i\blacksquare}$ to a three-dimensional neighbourhood of $\Gamma_{i\blacksquare}$.

The kernel $\mathbf{curl}_{\Gamma_{pq},\boldsymbol{x}} \Phi_{\kappa_i}(\boldsymbol{r})$ has – like the double layer kernel – a strong singularity $\mathcal{O}(\frac{1}{\|\boldsymbol{x}-\boldsymbol{y}\|^2})$ ($d = 3$). Therefore, the integrals are defined only as principal part integrals (see [33, Sect. 3.3.4]). Due to the jump relations (see [33, Thm. 3.3.1]) we know that no jump terms will occur. The kernel $\Phi_{\kappa_i}(\boldsymbol{r})$ in the second term of the identity above (see [33, Sect. 3.3.2]) has a weak singularity only. Moreover, since we choose $\widetilde{b}^j_{i\blacksquare}$, $j \in \{1, \ldots, M_{i\blacksquare}\}$ to be a basis of $\widetilde{V}_M \subset H^1(\partial\Omega_{\blacksquare})$, the integrals in (5.7) are well-defined in L^2.

5.4 Boundary Element Discretisation

5.4.1 Boundary Element Spaces

In contrast to classical Galerkin BEM, where we deal with discrete subspaces of the single-trace space $\boldsymbol{\mathcal{ST}}(\Sigma)$ and therefore face continuity requirements, in $\boldsymbol{\mathcal{L}}^2(\Sigma)$ we only need to make sure that the set of basis functions is $\boldsymbol{\mathcal{L}}^2(\Sigma)$-stable.

We already introduced the notation for finite dimensional subspaces of $\boldsymbol{\mathcal{L}}^2(\Sigma)$ in (5.2). In this chapter, our choice for V_M are conventional discontinuous polynomial boundary element trial and test spaces

$$V_M := \boldsymbol{\mathcal{L}}^2_{\mathcal{T}}(\Sigma) := \mathcal{S}^{p,-1}_{\mathcal{T}}(\Sigma) \times \mathcal{S}^{p,-1}_{\mathcal{T}}(\Sigma) \tag{5.8}$$

(see [33, Def. 4.1.17] ($d = 3$), [34, Sect. 10.2] ($d = 2$)). In other words, we consider piecewise polynomial functions of maximal total degree p with respect to a finite partition/triangulation $\mathcal{T} = \{\tau_1, \ldots, \tau_{|\mathcal{T}|}\}$ of Σ (see [33, Sect. 4.1.2]) that resolves the given geometry of Σ, in the sense that the closure of every Γ_{ij} agrees with the union of some closed cells of $\mathcal{T}$.

Since we are going to present numerical experiments based on piecewise constant boundary elements, in the sequel we restrict ourselves to $p = 0$. In addition, we will use mapped continuous piecewise linear boundary elements $\mathcal{S}^{1,0}_{\mathcal{T}}(\Sigma)$ (see [33, Def. 4.1.36] (d=3), [34, Sect. 10.2] ($d = 2$)).

5.5 Convergence and Conditioning

Take a shape-regular and quasi-uniform sequence $\{\mathcal{T}_\ell\}_{\ell\in\mathbb{N}}$ of skeleton meshes with

$$h_\ell := \max\{\operatorname{diam}(\tau),\, \tau \in \mathcal{T}_\ell\} \to 0 \text{ as } \ell \to \infty\,,$$

see [34, Section 10.1] ($d = 2$) or [33, Section 4.1.2] ($d = 3$) for details. Under these circumstances we find well-known interpolation error estimates for piecewise constant boundary element spaces, see [34, Theorem 10.4] ($d = 2$) or [33, Corollary 4.1.34] ($d = 3$). The approximation error estimates for continuous piecewise linear boundary element spaces can be found in [34, Theorem 10.9] ($d = 2$) or [33, Proposition 4.1.51] ($d = 3$).

Since it can only be shown that Formulation 3.3 is of the form "boundedly invertible+compact", we need to assume that discrete inf-sup conditions hold for the considered finite dimensional subspaces.

Assumption 5.1 (Discrete Inf-Sup Conditions) *We assume that Formulation 3.3, discretised by means of low-order piecewise polynomial boundary element spaces on shape-regular sequences of meshes, satisfies a uniform discrete inf-sup condition (see [33, Theorem 4.2.7]).*

Then, we conclude by [33, Theorem 4.2.7] well posedness, asymptotic stability, and quasi-optimality of the Galerkin discretisation. Quasi-optimality leads to $\mathcal{O}(h_\ell)$ algebraic convergence of the discretisation error in $\boldsymbol{\mathcal{L}}^2(\Sigma)$-norm by the interpolation error estimates [34, Section 10.1] or [33, Section 4.1.2], as long as the Cauchy traces of the solution belong to H^1 on each interface.

For $\mathcal{S}^{0,-1}_{\mathcal{T}_\ell}(\Sigma)$ we choose the "canonical" basis of characteristic functions of mesh cells, ordered in such a way, that it respects the interface-wise structure (see also (5.2))

$$\bigcup_{\Gamma_{ij}\subset\Sigma} \left\{b^1_{ij,\ell},\dots,b^{M_{ij,\ell}}_{ij,\ell}\right\} := \bigcup_{\Gamma_{ij}\subset\Sigma} \{|\tau|^{-\frac{1}{2}}\chi_\tau : \tau \in \mathcal{T}_\ell \cap \Gamma_{ij}\}\,. \tag{5.9}$$

This basis is perfectly L^2-stable, since it is even L^2-orthonormal.

Thus, by the continuity of $\mathbf{M}_\Sigma : \boldsymbol{\mathcal{ML}}^2(\Sigma) \to \boldsymbol{\mathcal{ML}}^2(\Sigma)$ and assuming that Assumption 5.1 holds true, we can conclude that for ℓ big enough the Euclidean condition numbers $\operatorname{cond}_2(\mathbf{G}_\ell)$ of the Galerkin matrices

$$\mathbf{G}_\ell \in \mathbb{C}^{M_\ell+\sum_{N\geq i>j\geq 0} M_{ij,\ell}, M_\ell+\sum_{N\geq i>j\geq 0} M_{ij,\ell}}$$

arising from the generalised case of Formulation 4.1 based on the space $V_M := \boldsymbol{\mathcal{L}}^2_{\mathcal{T}_\ell}(\Sigma)$ (see (5.8)), equipped with the basis given in (5.9), are bounded independently of ℓ.

5.6 Postprocessing

Assume that we solve the Linear System of Equations 5.1 using piecewise constant boundary element space $\mathcal{S}^{0,-1}_{\mathcal{T}}(\Sigma)$ as test and trial space on quasi-uniform meshes. In this case, we observe a gain in accuracy if we do a simple

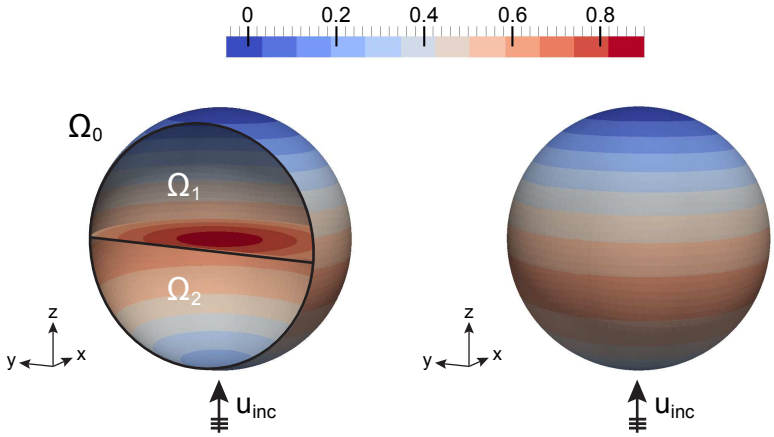

Fig. 6.1: Geometry of the scatterer in experiment I. Shown is the real part of the total field.

and cheap postprocessing. We apply a L^2-projection of the Dirichlet part of the discrete solution onto the continuous piecewise linear boundary element space $\mathcal{S}_{\mathcal{T}}^{1,0}(\Sigma)$. Assume that our computed solution is represented with respect to the canonical basis in (5.9) and that the coefficients of the calculated Dirichlet data are given by $\mathbf{u}_{D,0}$. Let $\mathbf{u}_{D,1}$ denote the expansion coefficients of the projected discrete solution wrt. to the continuous piecewise linear nodal shape functions spanning $\mathcal{S}_{\mathcal{T}}^{1,0}(\Sigma)$. Then, L^2-projecting means that we solve

$$\mathbf{M}_{11}\mathbf{u}_{D,1} = \mathbf{M}_{10}\mathbf{u}_{D,0}\,,$$

with $\mathbf{M}_{11}$ representing the mass matrix for continuous piecewise linear test and trial space and $\mathbf{M}_{10}$ characterizing the mass matrix for continuous piecewise linear test and piecewise constant trial space.

6 Numerical Experiments

This section is dedicated to numerical experiments testing the performance of our second-kind formulation compared to the classical first-kind formulation (see [35]) for $d = 3$.[5] While for the second-kind approach, we use piecewise constant boundary element test and trial space (see (5.8)), for the first-kind approach we need to use a $\boldsymbol{\mathcal{ST}}(\Sigma)$-conforming boundary element space. We take the space of continuous piecewise linear boundary elements $\mathcal{S}_{\mathcal{T}}^{1,0}(\Sigma)$ to discretise Dirichlet data and $\mathcal{S}_{\mathcal{T}}^{0,-1}(\Sigma)$ for Neumann data, respectively. The meshes we used for the experiments consisted of flat triangular cells.

[5] The implementation was done based on the C++ BEM library "Boundary Element Template Library 2" (BETL2), developed by L. Kielhorn [23].

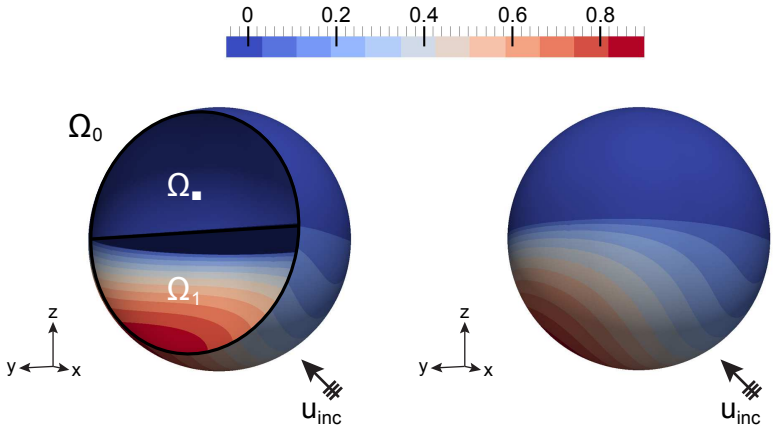

Fig. 6.2: Geometry of the scatterer in experiment II. Shown is the real part of the total field.

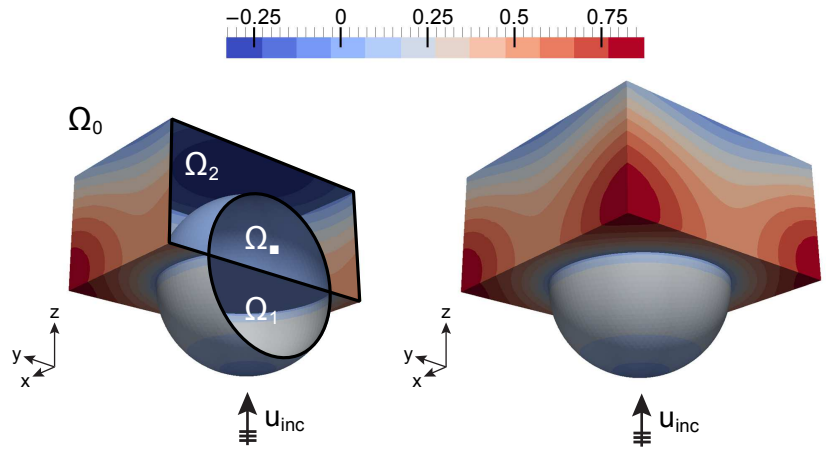

Fig. 6.3: Geometry of the scatterer in experiment III. Shown is the real part of the total field.

We are going to discuss three different scattering problems based on the geometries depicted in Figures 6.1, 6.2 and 6.3, respectively.[6]

[6] The meshes were generated with gmsh [16] and for visualisation of the computed data (see Fig. 6.1, 6.2, 6.3) we used ParaView [1]. All other plots were generated with MATLAB.

6.0.1 Experiment I: Transmission Problem

The first experiment solves the scattering problem (1.2a), (1.2b) at the composite scatterer shown in Figure 6.1 for the incident plane wave

$$U_{\text{inc}}(\boldsymbol{x}) = \exp(\mathrm{i}\kappa_0 \, \boldsymbol{d} \cdot \boldsymbol{x}) \,, \tag{6.1}$$

with direction of propagation $\boldsymbol{d} := (0,0,1)^\top$.
The scatterer consists of two different materials. The first part of the scattering obstacle is given by the ball $\mathcal{B}_{0.5}(\mathbf{0})$ of radius $r = 0.5$, centered in $\mathbf{0}$ and halved by the plane

$$\mathcal{E} := \{\boldsymbol{x} = (x,y,z)^\top \in \mathbb{R}^3 \,:\, z = 0\} \,.$$

The upper half of the ball in Figure 6.1, i.e.

$$\Omega_1 := \mathcal{B}_{0.5}(\mathbf{0}) \cap \{\boldsymbol{x} = (x,y,z)^\top \in \mathbb{R}^3 \,:\, z > 0\} \,,$$

is filled with a penetrable medium characterised by the wave number $\kappa_1 = 5$. The lower half of the ball, denoted by

$$\Omega_2 := \mathcal{B}_{0.5}(\mathbf{0}) \cap \{\boldsymbol{x} = (x,y,z)^\top \in \mathbb{R}^3 \,:\, z < 0\} \,,$$

is also penetrable and with wave number $\kappa_2 = 1$. The exterior domain

$$\Omega_0 := \mathbb{R}^3 \setminus \overline{\mathcal{B}_{0.5}(\mathbf{0})}$$

has wave number $\kappa_0 = 2$.

6.0.2 Experiment II: Transmission Problem with Impenetrable Part

We solve the acoustic scattering problem with incident plane wave (6.1) from direction $\mathbf{d} = \frac{1}{\sqrt{2}}(0,1,1)^\top$ hitting a ball-shaped scattering object $\mathcal{B}_{0.5}(\mathbf{0})$ of radius $r = 0.5$, centered at the origin. A picture of the geometry is given in Fig. 6.2. We impose homogeneous Dirichlet boundary conditions on $\partial\Omega_{\blacksquare}$, where

$$\Omega_{\blacksquare} := \mathcal{B}_{0.5}(\mathbf{0}) \cap \{(x,y,z)^\top \in \mathbb{R}^3 \,:\, z > 0\} \,.$$

The other half of the ball,

$$\Omega_1 := \mathcal{B}_{0.5}(\mathbf{0}) \cap \{(x,y,z)^\top \in \mathbb{R}^3 \,:\, z < 0\} \,,$$

is penetrable and characterised by $\kappa_1 = 4$. The exterior domain

$$\Omega_0 := \mathbb{R}^3 \setminus \overline{\mathcal{B}_{0.5}(\mathbf{0})}$$

has the wave number $\kappa_0 = 2$.

6.0.3 Experiment III: Complex Transmission Problem with Impenetrable Part

The incident plane wave (6.1) in Experiment III is incoming from direction $\mathbf{d} = (0,0,1)^\top$. The scatterer, which is depicted in Figure 6.3, consists of three different materials. The first part of the scattering obstacle is given by the ball $\mathcal{B}_{0.5}(\mathbf{0})$, with

$$\Omega_\blacksquare := \mathcal{B}_{0.5}(\mathbf{0}) \cap \{(x,y,z)^\top \in \mathbb{R}^3 \,:\, z > 0\}\,,$$

and

$$\Omega_1 := \mathcal{B}_{0.5}(\mathbf{0}) \cap \{(x,y,z)^\top \in \mathbb{R}^3 \,:\, z < 0\}\,.$$

$\Omega_\blacksquare$ is impenetrable and characterised by homogeneous Dirichlet boundary conditions on $\partial\Omega_\blacksquare$, while Ω_1 is a penetrable medium characterised by $\kappa_1 = 1$. In addition, we consider another medium given through $\kappa_2 = 4$ in

$$\Omega_2 := \mathcal{Q} \setminus \overline{\mathcal{B}_{0.5}(\mathbf{0})}\,,$$

where $\mathcal{Q} := \{(x,y,z)^\top \in \mathbb{R}^3 \,:\, 0.7 < x < -0.7\,,\ 0.7 < y < -0.7\,,\ 0.7 < z < 0\,\}$. The exterior domain

$$\Omega_0 := \mathbb{R}^3 \setminus \overline{(\mathcal{B}_{0.5}(\mathbf{0}) \cup \mathcal{Q})}$$

is penetrable with wave number $\kappa_0 = 2$.

6.1 Convergence and Post-Processing

We consider a sequence of nested meshes $\{\mathcal{T}_\ell\}_{\ell=1}^H$ with $H = 5, 6$. The corresponding number of elements are $\{44, 176, 704, 2816, 11264\}$ for Experiment I, $\{44, 176, 704, 2816, 11264, 45056\}$ for Experiment II, and $\{140, 560, 2240, 8960, 35840\}$ for Experiment III. They are created by uniform refinement and consist of flat, uniformly shape regular triangular elements. The local mesh width is calculated as the maximal distance of the center of mass to all points lying inside of the element. The global mesh width h_ℓ is given by the maximum over all local mesh widths. In Figure 6.4, we show the convergence of the of the error in $L^2(\Sigma)$ resp. $H^{-\frac{1}{2}}(\Sigma)$-norm with respect h_ℓ. As a reference solution we use the discrete solution calculated with the second-kind formulation on the finest grid $\mathcal{T}_H$. The convergence rates are as expected.

The term "proj. Dirichlet second-kind" denotes a post-processed version of the Dirichlet data of the second-kind solution, obtained by projecting the computed data onto the space of continuous piecewise linear boundary elements $\mathcal{S}^{1,0}_{\mathcal{T}}(\Sigma)$ in the L^2-sense (see Subsection 5.6).

The convergence plot in Figure 6.4 shows that the application of this cheap post-processing technique improves the convergence rate and we observe results that are as good as the results of the classical first-kind approach.

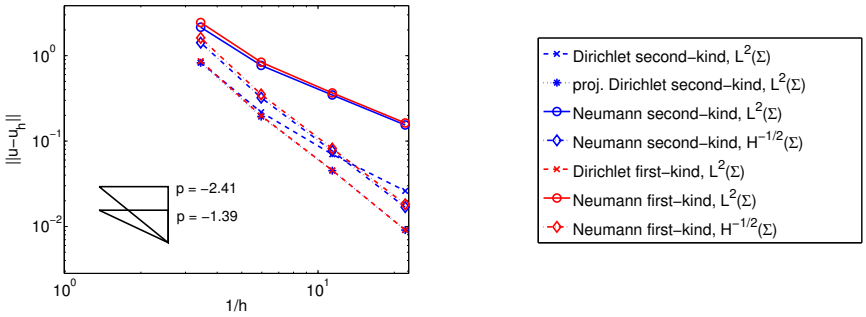

(a) Experiment I

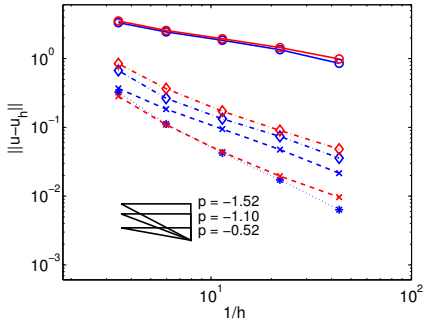

(b) Experiment II

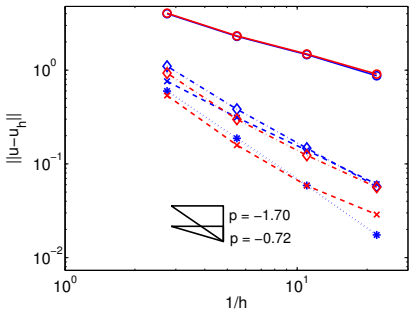

(c) Experiment III

Fig. 6.4: Convergence of the error of (diagonally rescaled) first- and second-kind Galerkin discretisation in L^2- and $H^{-\frac{1}{2}}$-norm for a sequence of meshes.

6.2 Conditioning of Galerkin Matrices

In Figure 6.5 the Euclidean condition number of the Galerkin matrices is plotted with respect to the inverse of the mesh width h_ℓ of the discretisation. As expected from the L^2-stability of the basis functions used for our second-kind Galerkin approximation (see (5.9)), we observe condition numbers for the Galerkin matrix that are almost independent of the mesh size, while the condition numbers of the Galerkin matrices of the first-kind approach blow up like $\mathcal{O}\left({h_\ell}^{-2}\right)$ (see Figure 6.5, compare with [33, Section 4.5 & Cor. 6.4.14]). This behaviour is directly reflected by the iteration count for the iterative solver GMRES, as can be seen in Figure 6.6.

6.3 Spurious Resonances Due to Impenetrable Objects

In this section, we are interested in what happens with the condition numbers of the Galerkin matrices in the case of spurious resonances. In the case of a

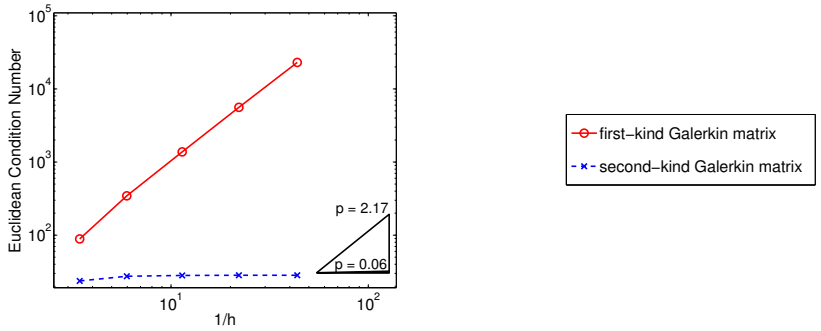

(a) Experiment I

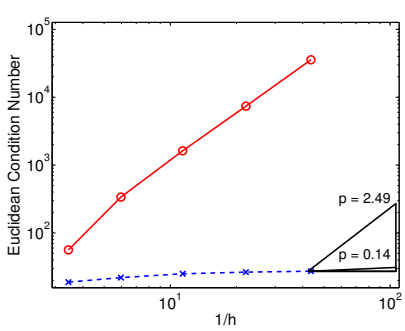

(b) Experiment II

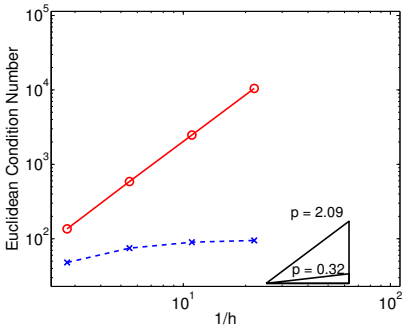

(c) Experiment III

Fig. 6.5: Condition numbers of (diagonally rescaled) first- and second-kind Galerkin matrices for a sequence of meshes.

single uniform ball-shaped scatterer $\Omega_{\blacksquare} := \mathcal{B}_r(\mathbf{0})$, we can explicitely compute the wave numbers for which we will observe a spurious resonance (see also Section 4). They correspond to the roots of derivatives of spherical Bessel functions and the roots of the spherical Bessel functions, respectively, scaled by $\frac{1}{r}$.

We take $r = 0.5$ and have a look at the range of wave numbers between 8.8 and 9.2. This range includes 8.986, which corresponds to $\frac{1}{r}x$, where $x = 4.493$ is the first root of the spherical Bessel function j_1 and the second root of the derivative of the spherical Bessel function j_0. Figure 6.7a shows the Euclidean condition numbers of the Galerkin matrices. Since we are computing the Galerkin matrices only at moderately fine meshes consisting of 512 and 2240 elements, we observe a shift of the resonance due to approximation errors. Obviously, the spurious resonances disappear when using a CFIE approach.

In addition to the simple ball-shaped scatterer $\mathcal{B}_{0.5}(\mathbf{0})$, we also consider the geometry depicted in Figure 6.3, taking the cuboid as pseudo-interface, i.e. setting $\kappa_2 = \kappa_0$, and defining Ω_1 to be impenetrable, too. In this setting, we get rid of the spurious resonances in the case of the first-kind formulation

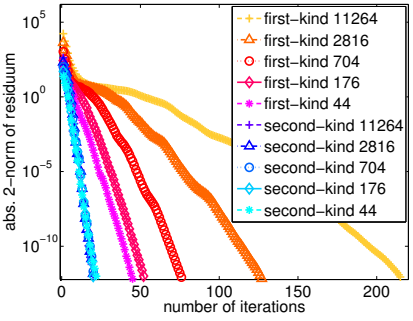

(a) Experiment I

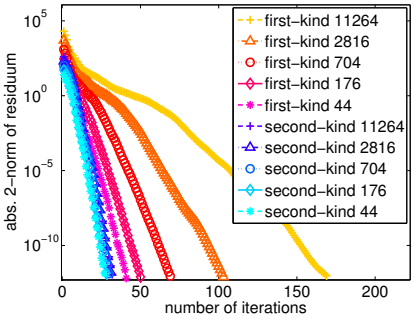

(b) Experiment II

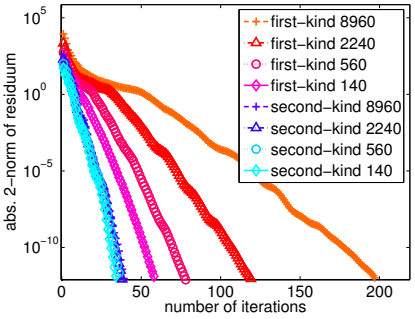

(c) Experiment III

Fig. 6.6: Performance of GMRES applied to (diagonally rescaled) first- and second-kind Galerkin system.

(see [8]). Unfortunately, in the case of the second-kind formulation, this effect is not observed. But nevertheless, the condition numbers for the first-kind formulation with pseudo-interface increase drastically such that it is not really an improvement to use pseudo-interfaces for first-kind formulations.

7 Conclusion

In this paper, we have extended the second-kind formulation in [11] to partly impenetrable scatterers and provided a combined-field approach to overcome spurious resonances due to the impenetrable parts. Numerical experiments show that our formulation is very competitive to the widely used classical first-kind approach [35]: our formulation is intrinsically well-conditioned and achieves accuracy comparable to the first-kind approach when applying a cheap post-processing technique. On the other hand, the first-kind formulation leads to ill-conditioned systems and therefore we observe poor convergence of iterative solvers.

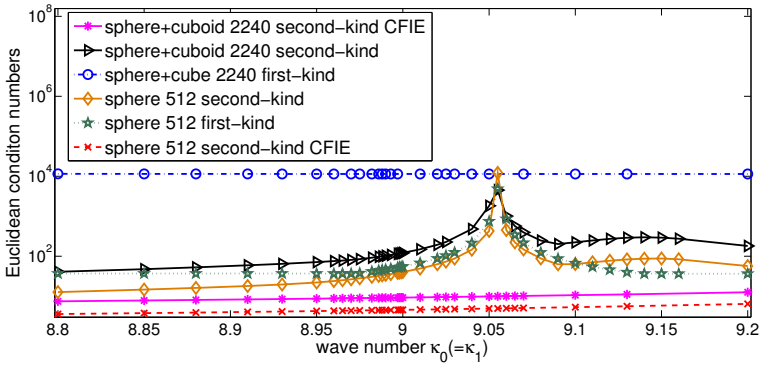

Fig. 6.7: Spurious resonances due to impenetrable objects: condition numbers of the first- and second-kind Galerkin matrix for various wave numbers, $\kappa_0 = \kappa_1$.

Acknowledgement

The authors would like to thank L. Kielhorn for his great support during the development of the code for the first- and second-kind formulation in BETL2 [23].

References

1. U. Ayachit. The ParaView Guide: A Parallel Visualization Application. *Kitware*, 2015.
2. J. M. Ball, Y. Capdeboscq, and B. T. Xiao. On uniqueness for time harmonic anisotropic Maxwell's equations with piecewise regular coefficients. *Math. Models Meth. Appl. Sci.*, 2012.
3. A. Buffa and R. Hiptmair. Regularized Combined Field Integral Equations. *Numerische Mathematik*, Springer Verlag, 100(1):1–19, 2005
4. A. J. Burton and G. F. Miller. The application of integral equation methods to the numerical solution of some exterior boundary-value problems. *Proceedings of the Royal Society of London A: Mathematical, Physical and Engineering Sciences*, 323(1553):201–210, 1971.
5. Y. Chang and R. Harrington. A surface formulation for characteristic modes of material bodies. *IEEE Transactions on Antennas and Propagation*, 25(6):789–795, 1977.
6. X. Claeys. A single trace integral formulation of the second kind for acoustic scattering. *Tech. Rep. 2011–14*, Seminar for Applied Mathematics, ETH Zürich, 2011.
7. X. Claeys and R. Hiptmair. Multi-trace boundary integral formulation for acoustic scattering by composite structures. *Communications on Pure and Applied Mathematics*, 66: 11631201, 2013.
8. X. Claeys and R. Hiptmair. Integral Equations for Acoustic Scattering by Partially Impenetrable Composite Objects. *Integral Equations Operator Theory*, 81(2): 151-189, 2015.
9. X. Claeys, R. Hiptmair, and C. Jerez-Hanckes. Multitrace boundary integral equations. Direct and Inverse Problems in Wave Propagation and Applications, *Radon Series on Computational and Applied Mathematics*, 14:51–100, 2013.
10. X. Claeys and R. Hiptmair and C. Jerez-Hanckes and S. Pintarelli. Novel Multi-Trace Boundary Integral Equations for Transmission Boundary Value Problems. *Unified Transform for Boundary Value Problems: Applications and Advances*, SIAM, 2015.

11. X. Claeys, and R. Hiptmair, and E. Spindler. A second-kind Galerkin boundary element method for scattering at composite objects. *BIT Numerical Mathematics*, 55(1):33-57, 2015.
12. D. Colton and R. Kress. Inverse Acoustic and Electromagnetic Scattering Theory. Vol. 93. *Springer Science & Business Media*, 2012.
13. M. Costabel and E. P. Stephan. A direct boundary equation method for transmission problems. *J. Math. Anal. Appl.*, 106:367–413, 1985.
14. M. Costabel and E. P. Stephan. Boundary integral equations for mixed boundary value problems in polygonal domains and Galerkin approximation. *Banach Center Publications*, 15(1):175–251, 1985.
15. J. Elschner. The double layer potential operator over polyhedral domains I: Solvability in weighted Sobolev spaces. *Applicable Analysis* 45(1-4):117–134, 1992.
16. C. Geuzaine and J.-F. Remacle. Gmsh: a three-dimensional finite element mesh generator with built-in pre- and post-processing facilities. *International Journal for Numerical Methods in Engineering*, 79(11):1309–1331, 2009.
17. L. Greengard and J.Y. Lee. Short note: Stable and accurate integral equation methods for scattering problems with multiple material interfaces in two dimensions. *Journal of Computational Physics*, 231(6):2389–2395, 2012.
18. P. Grisvard. Singularities in boundary value problems. *Recherches en mathématiques appliquées*, Masson, 1992.
19. R.F. Harrington. Boundary integral formulations for homogeneous material bodies. *J. Electromagnetic Waves and Applications*, 3(1):1–15, 1989.
20. C. Hazard and M. Lenoir. On the solution of time-harmonic scattering problems for Maxwell's equations. *SIAM J. Math. Anal.*, 27(6):1597–1630, 1996.
21. R. Hiptmair. Operator preconditioning. *Computers and Mathematics with Applications*, 52:699–706, 2006
22. R. Hiptmair and C. Jerez-Hanckes. Multiple traces boundary integral formulation for Helmholtz transmission problems. *Adv. Appl. Math.*, 37:39-91, 2012.
23. R. Hiptmair and L. Kielhorn. BETL - a generic boundary element template library. *Tech. Rep. 2012–36*, Seminar for Applied Mathematics, ETH Zürich, 2012.
24. D. Jerison and C. E. Kenig. The inhomogeneous Dirichlet problem in Lipschitz domains. *J Funct. Anal.*, 130(1):161-219, 1995.
25. R. Kress and GF Roach. Transmission problems for the Helmholtz equation. *Journal of Mathematical Physics*, 19(6):1433–1437, 1978.
26. W. McLean. Strongly Elliptic Systems and Boundary Integral Equations. *Cambridge University Press*, Cambridge, UK, 2000.
27. A.-W. Maue. Zur Formulierung eines allgemeinen Beugungsproblems durch eine Integralgleichung. *Zeitschrift für Physik*, 126(7-9):601–618, 1949.
28. C. Müller. Foundations of the mathematical theory of electromagnetic waves. *Springer Verlag*, 1969.
29. Z. Peng, K.-H. Lim, and J.-F. Lee. Computations of electromagnetic wave scattering from penetrable composite targets using a surface integral equation method with multiple traces. *IEEE Trans. Antennas and Propagation*, 61:256-270, 2013.
30. Z. Peng, X.-C. Wang, and J.-F. Lee. Integral equation based domain decomposition method for solving electromagnetic wave scattering from non-penetrable objects. *IEEE Trans. Antennas and Propagation*, 59:33283338, 2011.
31. A. J. Poggio and E. K. Miller. Integral equation solution of three-dimensional scattering problems. *Computer Techniques for Electromagnetics*, chapter 4, p. 159–263, New York, 1973.
32. V. Rokhlin. Solution of acoustic scattering problems by means of second kind integral equations. *Wave Motion*, 5(3):257–272, 1983.
33. S. A. Sauter and C. Schwab. Boundary element methods. *Springer Verlag*, 2011.
34. O. Steinbach. Numerical approximation methods for elliptic boundary value problems: finite and boundary elements. *Springer Verlag*, 2008.
35. T. Von Petersdorff. Boundary integral equations for mixed Dirichlet, Neumann and transmission problems. *Mathematical methods in the applied sciences*, 11(2):185–213, 1989.
36. T.-K. Wu and L. L. Tsai. Scattering from arbitrarily-shaped lossy dielectric bodies of revolution. *Radio Science*, 12(5): 709 – 718, 1977.

Recent Research Reports

Nr.	Authors/Title

2015-09 J.-L. Bouchot and B. Bykowski and H. Rauhut and Ch. Schwab
Compressed Sensing Petrov-Galerkin Approximations for Parametric PDEs

2015-10 A. Jentzen and P. Pusnik
Strong convergence rates for an explicit numerical

approximation method for stochastic evolution equations with

non-globally Lipschitz continuous nonlinearities

2015-11 R. Bourquin
Exhaustive search for higher-order Kronrod-Patterson Extensions

2015-12 R. Bourquin and V. Gradinaru
Numerical Steepest Descent for Overlap Integrals of Semiclassical Wavepackets

2015-13 A. Hiltebrand and S. Mishra
Entropy stability and well-balancedness of space-time DG for the shallow water equations with bottom topography

2015-14 B. Ayuso de Dios and R. Hiptmair and C. Pagliantini
Auxiliary Space Preconditioners for SIP-DG Discretizations of H(curl)-elliptic Problems with Discontinuous Coefficients

2015-15 A. Paganini and S. Sargheini and R. Hiptmair and C. Hafner
Shape Optimization of microlenses

2015-16 V. Kazeev and Ch. Schwab
Approximation of Singularities by Quantized-Tensor FEM